NOVA SCHOOL OF SCIENCE & TECHNOLOGY

MATERIALS DEPARTMENT

Guilherme Veríssimo Cândida

BSc in Materials Science

Mimicking bone structure with functionally graded auxetic structures

MASTERS IN MATERIALS ENGINEERING

NOVA University Lisbon

November, 2021

NOVA SCHOOL OF SCIENCE & TECHNOLOGY

MATERIALS DEPARTMENT

Guilherme Veríssimo Cândida

BSc in Materials Science

Mimicking bone structure with functionally graded auxetic structures

MASTERS IN MATERIALS ENGINEERING

NOVA University Lisbon

November, 2021

NOVA SCHOOL OF SCIENCE & TECHNOLOGY

MATERIALS DEPARTMENT

Mimicking bone structure with functionally graded auxetic structures

Guilherme Veríssimo Cândida

BSc in Materials Science

Adviser: João Paulo Miranda Ribeiro Borges
Associate Professor w/ Habilitation, NOVA University Lisbon

Co-advisers: Alexandre José da Costa Velhinho
Associate Professor, NOVA University Lisbon

Examination Committee:

Chair: Name of the committee chairperson,
Full Professor, FCT-NOVA

Rapporteurs: Name of a rapporteur,
Associate Professor, Another University
Name of another rapporteur,
Assistant Professor, Another University

Adviser: Name of the adviser present in defense,
Associate Professor, University

Members: Yet another member of the committee,
Full Professor, Another University
Yet another member of the committee,
Assistant Professor, Another University

MASTER IN MATERIALS ENGINEERING

NOVA University Lisbon
November, 2021

ACKNOWLEDGMENTS

Firstly, I would like to start by thanking my adviser and co-adviser, Prof. Doutor João Paulo Borges and Prof. Doutor Alexandre Velhinho for all the support and mentoring during this project, for their availability and for all the knowledge passed on during this journey.

Secondly, I would like to thank João Cardoso for his more personal involvement, accompaniment and also availability to provide feedback and a helping hand on every challenge.

Thirdly, I would like to thank my work colleagues, Gonçalo Catatão and Patrícia Almeida, especially Gonçalo, with whom I've had the pleasure of working side by side with every step of the way for the duration of this work, constantly exchanging ideas and finding solutions to the various problems encountered.

Last but not least, I'd like to thank my family, which always supported me, my friends, who made this academic journey a much more pleasant experience, and my girlfriend, who always stood by my side, believed in my abilities and played a crucial role in my development as a person, both personally and academically.

“Doubt is the beginning of wisdom.” (Aristotle).

ABSTRACT

Nowadays the golden standard in orthopedic implants for bone regeneration is the use of allografts and autografts. However, these present problems regarding the availability of the required tissue and risks related to surgery, immune system rejection and pathogen transmission. With the recent development of additive manufacturing, novel porous structures are being looked upon as a possible answer to the afore mentioned problems. In this study, a structure based on the gyroid triply periodic minimal surface was modelled, produced via the fused deposition modeling (FDM) 3D printing method, and mechanically characterized, with the aim of getting one step closer to obtaining bone mimicking implants.

Keywords: 3D printing, Auxetic, Bone regeneration, Computer modeling, Gyroid, Metamaterials

RESUMO

Atualmente, o arquétipo da regeneração óssea são os autoenxertos e aloenxertos. No entanto, estes enxertos ósseos apresentam desvantagens, tais como a disponibilidade limitada dos tecidos necessários e os riscos associados a cirurgias, rejeição imunológica e transmissão de agentes patogénicos. Com o recente desenvolvimento dos métodos de fabricação aditiva, novas estruturas porosas estão a ser contempladas como possíveis soluções para estes problemas. Neste estudo, foi modelada uma estrutura baseada na superfície mínima triplamente periódica giróide, que foi depois impressa em 3D e caracterizada mecanicamente, com o intuito de chegar um passo mais perto de obter implantes que imitem as propriedades mecânicas dos ossos.

Palavras chave: Auxético, Impressão 3D, Regeneração óssea, Giróide, Metamateriais, Modelação computacional

CONTENTS

LIST OF FIGURES

LIST OF TABLES

ACRONYMS

Al	Aluminum.
CAD	Computer-aided Design.
FDM	Fused Deposition Modeling.
L-PBF	Laser Powder Bed Fusion.
NC	Negative Compressibility.
PR	Poisson´s Ratio.
NPR	Negative Poisson´s Ratio.
NTE	Negative Coefficient of Thermal Expansion.
SDL	Standard Tesselation Language.
SLM	Selective Laser Melting.
Ti	Titanium.
TPU	Thermoplastic Polyurethane.
V	Vanadium.

SYMBOLS

π	Pi - Mathematical constant representing the ratio between a circle's perimeter and diameter, having a value rounded to eight decimal places of 3.14159265.
ν	Poisson's Ratio.
ε	Strain - Measure of the relative deformation of a body subjected to applied forces.

Motivation and Objectives

Additive manufacturing could be the basis for the next generation of implants incorporating metamaterials, promising to make them cheaper, safer and more widely available. The development and characterization of new such structures is important in order to reach ever higher levels of resemblance between bone and implant.

The main objectives of this study correspond to the design, manufacturing and mechanical behavior evaluation of a 3D functionally graded auxetic structure that can mimic long bone structure, and which has superior mechanical properties when compared to conventional scaffolds/implants.

1

INTRODUCTION

1.1 Poisson's ratio

Most materials, when stretched along a longitudinal direction, react by contracting in the transversal direction. The opposite also applies, where materials that are compressed along a longitudinal direction react by expanding in the transversal direction. This reaction is in line with the intuitive idea of a materials' conservation of volume. The Poisson's ratio (PR) is a dimensionless mechanical property of any given material, which can either be (for anisotropic materials) dependent or (in the case of isotropic materials) independent on the direction of an applied load, and which quantifies the ratio between the deformation along the transversal direction, and that which simultaneously occurs along the longitudinal direction; given that, for most materials, the two deformations have opposite signs, this ratio is by definition multiplied by a factor of -1 (1). The PR thus assumes positive values for the vast majority of materials [1]–[3].

$$\nu = -\frac{\varepsilon_{transversal}}{\varepsilon_{longitudinal}} \tag{1}$$

1.2 Bone grafts

Bone is one of the most transplanted tissues in clinics and hospitals worldwide. However, guiding bone regeneration (osteogenesis) via the treatments currently used is still far from perfect. As it is, autografts and allografts are the go-to ways of regenerating bone defects. These consist in no more than taking biological material from and into the same patient (autografts [4], [5]) or taking biological material from a donor and implanting it into the patient (allografts [4], [5]).

Autografts present good osteogenic properties such as osteoconductivity (the ability of bone forming cells to move freely across the scaffold) and osteoinductivity (the ability for bone forming cells to proliferate) and have a relatively small chance of immune rejection. However, its drawbacks are the quantity of tissue available and the requirement of performing two surgeries on the patient instead of just one, therefore increasing surgery related risks, and the possibility of donor-site morbidity where the tissue was removed. Allografts, on the other hand, require only one surgery to be performed and have less limited tissue availability, but have diminished osteogenic properties and an increased risk of immune rejection and pathogen transmission from donor to host [4], [5].

For these reasons, and with the development of additive manufacturing techniques with the capacity to create complex porous structures, 3D synthetic scaffolds with bone regeneration properties seem like a promising replacement to allografts and autografts, having the potential to eliminate most of these problems. The fact that they do not require human bone tissue and can therefore be easily mass produced, only require one surgery while not exposing the patient to risk of immune rejection or pathogen transmission, and can still provide good osteogenic properties, are some of the biggest benefits of using these structures [5].

Meanwhile, trabecular bone (highly porous bone located between the bone marrow and the denser, outer shell of the bone, the cortical bone) has been shown to display an auxetic behavior [6], which means that implanting a non-auxetic material for bone regeneration or substitution, will cause it to retract relative to the bone. This not only increases local stress and strain concentrations at the interfacial area between the implant and the internal bone surfaces, but also leads to inferior implant fixation due to lack of mechanical stimuli and allows wear particles into the bone-implant interface, which might lead to premature mechanical failure in this area and therefore inefficacy of the implant. Also, due to the inherently porous nature of

auxetic structures, these display lower stiffnesses than those found in conventional implants, which helps reduce the stress-shielding effect [7]–[9].

The use of metamaterials in orthopedic applications has already been studied for improving the longevity of total hip replacement implants. A series of publications have been released on the creation of a new type of implant, composed of a mixture of a conventional and an auxetic material with a hexagonal reentrant geometric structure. The structures were fabricated using a Ti–6Al–4V alloy, a commonly used material for bone replacement implants, via selective laser melting (SLM) [8], [9].

These structures aim to improve the implant-bone interface, reducing mechanical failure in that area and increasing bone growth, therefore reducing the penetration capacity of wear particles between the bone and the implant, and increasing implant longevity. Multiple structures were produced, with varying ratios of conventional and auxetic material, and their mechanical properties were studied using compression tests [8], [9].

These studies highlight the limitations imposed by the additive manufacturing techniques in the resulting auxetic materials' properties, namely regarding its resolution and the need for the use of a support inside the porous structure, as certain designs had to be abandoned due to being outside the processability window of the SLM process [8], [9].

Furthermore, a recent study has been conducted on the use of the gyroid geometry to create titanium sheet scaffolds meant for repairing critically sized femoral bone defects (Figure 1). The scaffolds were made using the same Ti–6Al–4V alloy, produced using laser powder bed fusion (L-PBF), and recombinant bone morphogenic protein-2 was added, to assess the effect of pore size in the treatment of rats' femoral critical size bone defects and its osteogenic capacities.

The additive manufacturing method proved to be a limitation as the printed structure was deviated from the CAD model, displaying less porosity than desired. Small pore scaffolds were found to be more stable as they did not suffer any misalignments with the cortical bone, and therefore displayed very good mechanical properties, at the cost of inferior bone regeneration properties. Large pore scaffolds displayed superior osteogenic properties but were found to be misaligned with the cortex, reducing their mechanical properties [10].

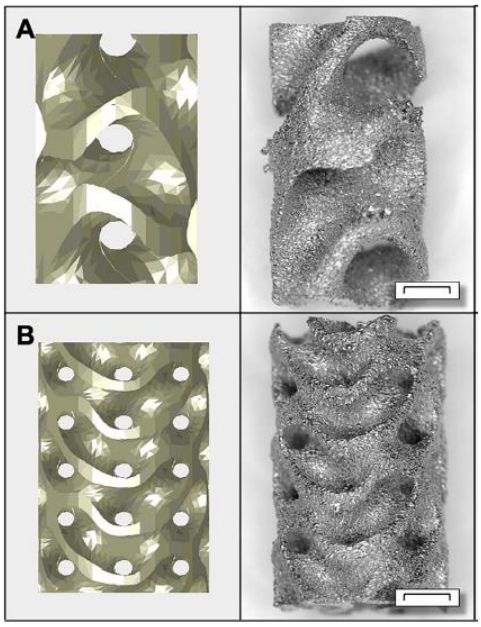

Figure 1 - CAD renderings (left) and images of the produced scaffolds (right) of large pore (A) and small pore (B) gyroid-sheet structures. The scale bars represent 1 mm.

1.3 Auxetic metamaterials

Metamaterials are materials that display anomalous or counter intuitive mechanical properties, mostly due to their geometric structure rather than composition [11]. Examples of metamaterials are auxetic metamaterials, materials with a negative coefficient of thermal expansion (NTE), anepectic metamaterials and materials with negative compressibility (NC). Auxetic materials display a negative Poisson's ratio (NPR) [12], materials with a NTE shrink as their temperature rises [13], anepectic materials display both a NPR and a NTE [14], [15], and materials with negative compressibility transition respond to increasing hydrostatic pressures by expanding, rather than shrinking [16].

Auxetic materials have been known to exist for at least 150 years [17]. In 1892, Prof. Voigt of Göttingen came to prove the existence of such behavior in pyrites, in his experiments on the torsion and flexure of rods [18]. Other natural and also synthetic materials have since been studied and found to have a NPR, such as polymorphic silicones [19], silicates [20], zeolites [21], [22], fibers in general [23], biological tissues, including cancellous or trabecular bone [6], metal-organic frameworks, graphene, carbon nanotubes, foams, polymers, and perforated systems [1], [11], [17].

However, natural auxetic materials are scarce and typically difficult to assign to a specific practical application [1]. As such, attempts at synthesizing this behavior in a controlled manner

begun, resulting in the first ever synthetic auxetic material, a polyester foam, being fabricated in 1987, by Roderic Lakes [3].

This type of metamaterial has been attracting more and more attention as they exhibit improved characteristics, mechanical, optical or acoustic, when compared to conventional materials, such as the ability to undergo synclastic curvature [3], [11], [12], [24], their increased indentation resistance [3], [11], [12], [24], shear resistance [1], [12], [24], [25] and fracture toughness [1], [12], [17], variable permeability with strain [1], [12], [25], excellent energy absorption [12], [24]–[26] and sound dampening properties (for auxetic foams) [1], [11], [16], [24], all while having reduced weight [26], making them suitable in a number of applications such as biomedicine [8], [10], [27], sensors [25], [26], electronics [11], aerospace [12], [25], civil and aeronautical engineering [24], vehicle crashworthiness [24], body armor [24], [25] and others.

The main challenge faced when trying to implement the use of auxetic materials in any given application is the limitation imposed by the current production methods [17]. The need to obtain a porous geometric structure with very specific dimensions requires the use of additive manufacturing techniques, such as laser powder bed fusion (L-PBF) [10], selective laser melting (SLM) [8], [26], FDM [24], laser lithography, 3D printing, molding and perforation methods [11], but these are highly dependent on the specific geometric features and desired materials of each structure. These techniques allow the user to obtain tailor made material properties but are limited in precision and in the number of different materials they are each able to process.

1.4 Gyroid structure

The gyroid structures have come to light recently as auxetic structures with increased interest for biomedical applications due to its high permeability and curvature similar to that of trabecular bone, as well as for its superior heat transfer and energy absorption properties. It is a triply periodic structure meaning that it can be scaled up simply by copying its basic unit in all three directions (Figure 2). The structure has been observed naturally in wings of butterflies and intercellular membranes [10], [28].

It is defined by the mathematical function (2) [28]:

$$\sin\left(\frac{2\pi x}{a}\right).\cos\left(\frac{2\pi y}{a}\right)+\sin\left(\frac{2\pi y}{a}\right).\cos\left(\frac{2\pi z}{a}\right)+\sin\left(\frac{2\pi z}{a}\right).\cos\left(\frac{2\pi x}{a}\right)=t \qquad (2)$$

Figure 2 - MATLAB generated gyroid structures as seen from a [100] plane perspective and a [111] perspective.

1.5 Additive manufacturing - FDM

Fused deposition method (FDM) is a technique where a virtual computer assisted design (CAD), made using a specialized software, is fabricated by depositing layer upon layer of extruded thermoplastic material, which is heated beyond its melting point and deposited onto a substrate. To fabricate a porous structure, one can use direct FDM and indirect FDM. Direct FDM fabricates the structures as they are meant to be, whereas indirect FDM fabricates the mold for the structure, which can then be infiltrated with the desired material and removed [4].

This process is widely used in biomedical engineering applications, but also for breathing apparatus as face shields, as a replacement for casting, to make customized house and building designs, plane prototypes, automotive parts, among others [23].

Its versatility and the fact that it is inexpensive has also made it suitable for aerospace applications, such as in the printing of space rover parts in thermoplastic materials like ABS, PCABS and polycarbonates, producing plastic parts strong enough to replace metal parts, while reducing weight [29].

In order to overcome an incompatibility between a geometric structure and a given additive manufacturing process, one must find an alternative design that better suits the available manufacturing technique, while maintaining its desired auxetic behavior and the properties that come along with it. New geometries have been and continue to be developed to reduce complications in the manufacturing process of these materials. Some examples of 2D and 3D auxetic structures are star-shaped [11], hexagonal reentrant or honeycomb reentrant [1], [17], [30], double arrowhead [24], latitude-and-longitude-inspired [31] and gyroid geometries [10], [26], [28], the rotating rigid and semi-rigid deformation model [1], [32], [33], chiral structures [1], [32], [33] and foams [3], [17], [32].

2

MATERIALS AND METHODS

In this chapter the design, manufacturing process and characterization of the structures will be described. A more detailed description can be found in Annex A.

All structures were 3D printed in commercially available thermoplastic polyurethane (Ultimaker TPU 95A) filament through FDM. TPU being an elastic material, it was chosen with mechanical testing in mind, to allow for better observation of how said structures deform when compressed up to high levels of strain.

2.1 Gyroid surface

The gyroid surface was generated and then exported in .stl format using the MATLAB programming platform (MATLAB R2019a) and the equation that describes it (2).

A MATLAB code was made specifically to generate this surface, using the gyroids' mathematical equation. It can be found in Annex A.

2.2 Structure modelling

After generating the gyroid surface in MATLAB and exporting it in .stl format, it was then loaded into the 3D modelling software Blender.

In Blender, two different types of structures were modeled. Firstly, a series of 7 cubic shaped gyroid based structures, with 36.9 mm in side, each with a different wall thickness, were modeled in order to assess the impact that the wall thickness has on the structures PR. Secondly, six tube-shaped Gyroid like structures aimed to mimic bone morphology were modeled, with different inner diameters and different thickness gradients, to assess the impact

of the size of the hollow region in the middle of the structure, as well as the range of thicknesses, in its mechanical properties.

The cubes were modeled by simply loading the gyroid surface from MATLAB and applying a solidify modifier to it with the specified desired thickness, and finally trimming it with a regular cube to make a smooth surface for mechanical testing, using the Boolean modifier.

To model the cylindrical structures, a linear thickness gradient was applied roughly in the middle section of the structure by making use of the weight paint tool and the solidify modifier. Subsequently, the structure was trimmed, again to create a smooth surface and facilitate mechanical testing, using the Boolean modifier. Finally, a tube-shaped structure with a hole in the middle was generated by first applying an array modifier on the resulting structure and then a curve modifier which bends the array along the shape of a circle with the desired dimensions (Figure 3). Again, a more detailed description can be found in Annex A.

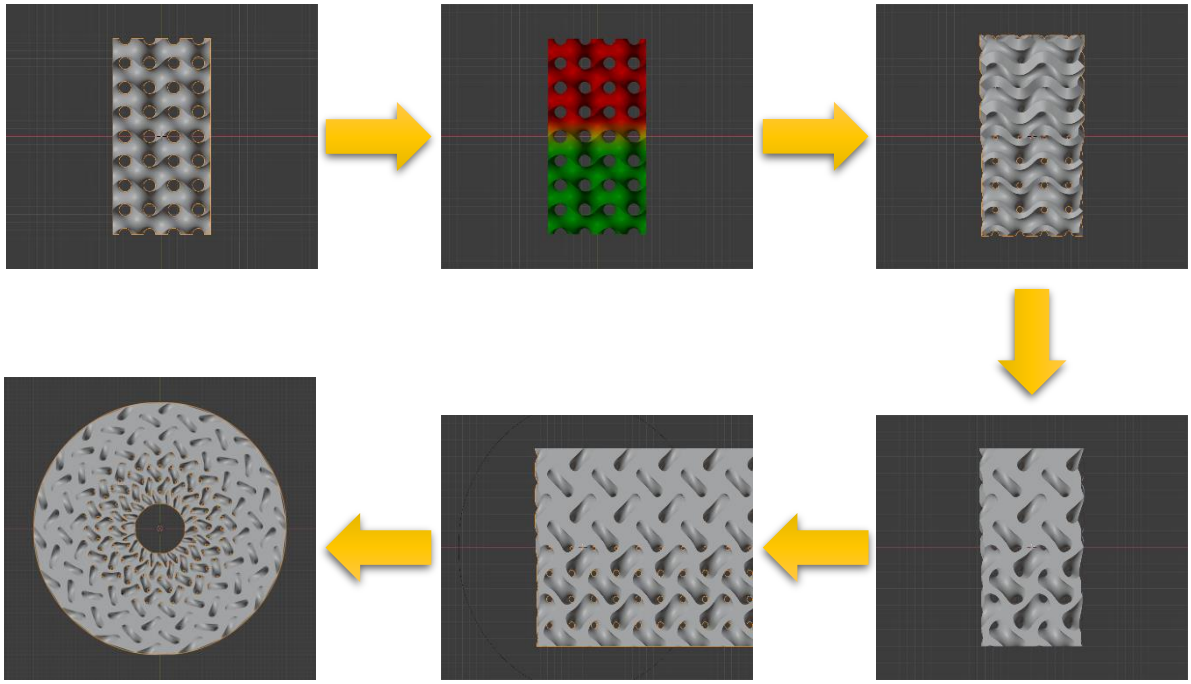

Figure 3 - Schematic of the modelling process used for obtaining bone mimicking structures based on the gyroid surface

The structure is then exported in .stl format, which can be loaded on the software Cura.

2.3 3D printing

The structures exported from Blender were loaded into the slicing software Cura, sliced and printed in an Ultimaker 3 FDM printer. It then exports the result in .gcode format, which can then be read by the printer via a USB pen.

2.4 Mechanical testing

All samples were subjected to compression testing in a Shimadzu AG-50kN G universal testing machine. All tests were performed up to 50% strain, at a speed of 1.6 mm/s for all cubic samples and 1.3 mm/s for all cylindrical samples. All tests were filmed using a Canon EOS 2000D camera to determine their PR. The camera can only film continuously for 12 minutes, hence the different test speeds.

2.5 Characterization

To obtain the structures' stress/strain curves and PR, as well as other useful data on the deformation of the structures, a MATLAB program was adapted from G. Catatão's study [34] and used. In order to determine the PR, a series of red dots were painted on the structures by hand, 16 dots for the cubic samples, and 13/23 dots for the cylindrical samples, using bright red varnish. These dots were then reinforced with a layer of matting agent, to reduce light reflection on their surface.

The program recognizes these red dots through their RGB indexes, and tracks their positions between frames, turning distance between them into strain both in the longitudinal direction as well as the transversal direction, allowing for the determination of the PR.

3

RESULTS AND DISCUSSION

3.1 Full infill TPU cube

For comparison purposes, a compact 2x2x2 cm TPU cube was printed (Figure 4). It was also used to empirically determine the density of the TPU filament. The cube weighed 9.5831±0.0001 g, resulting in a filament density of 1.2 g/cm^3.

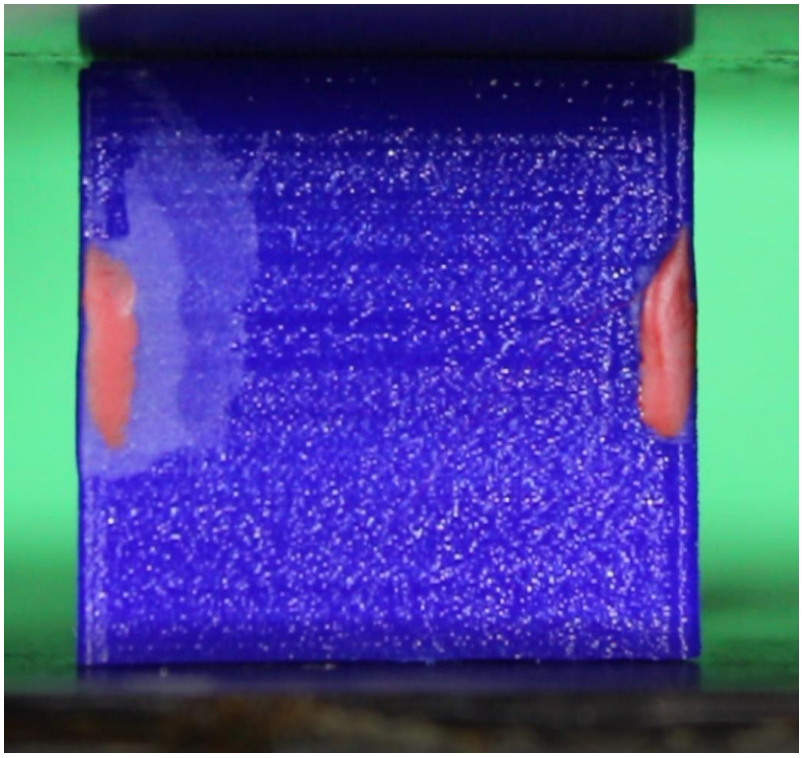

Figure 4 - Compact TPU cube

The cubes' Stress-Relative displacement (Figure 5) and PR-Relative displacement (Figure 6) curves were obtained using MATLAB. Its elasticity modulus was determined to be 43.917 MPa by doing a linear fit on its Stress-Relative displacement curve, and extracting the value of its slope. Its PR values are high, varying from around 0.3 up to 0.7. Relative displacemente refers to the movement of the top plate relative to the samples' height.

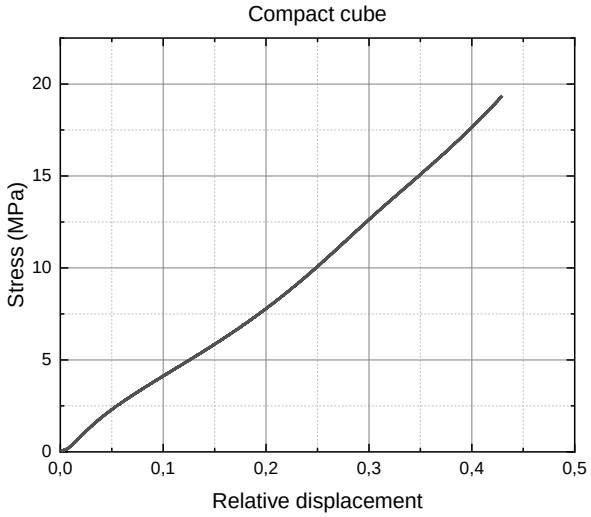

Figure 5 - Stress / Relative displacement curve of the compact TPU cube

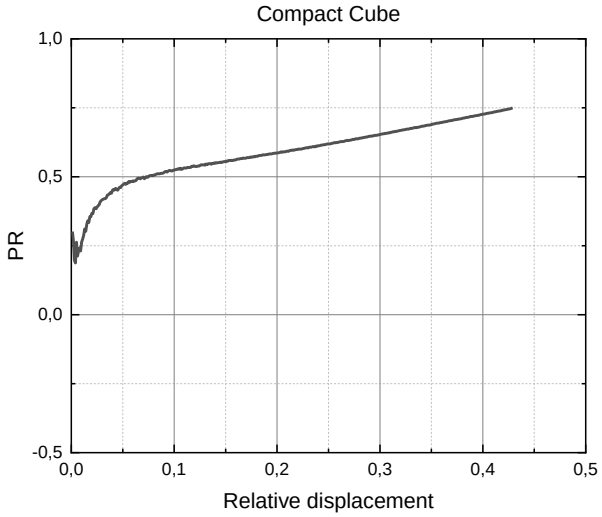

Figure 6 - PR / Relative displacement curve of the compact TPU cube

3.2 Cubic Gyroid structures

A total of 21 cubic shaped structures based on the gyroid surface were produced, organized by thickness in 7 groups (Figure 7), from 1.5 to 6 mm in steps of 0.75 mm, with 3 samples in each group. The porosity of the structure for each wall thickness was also determined (Table 1). They were then subjected to compression testing and analyzed to determine their PR.

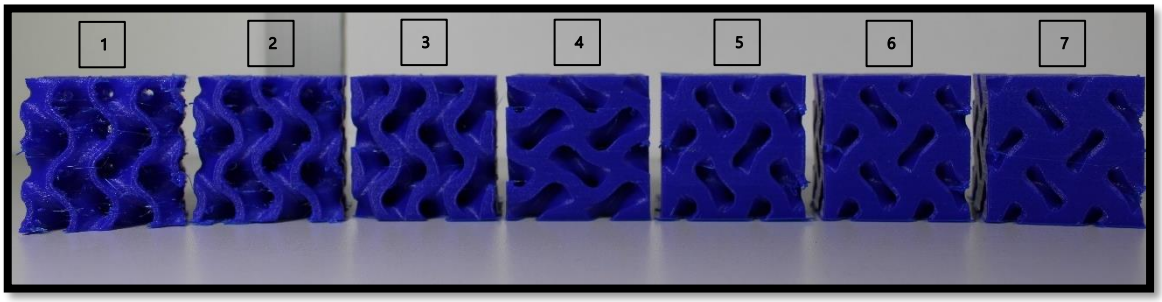

Figure 7 - Cubic shaped gyroid structures ordered by increasing wall thickness, the lowest being 1.5 mm thick (1), and increasing in steps of 0.75 mm up to the highest wall thickness of 6 mm (7).

	1.5 mm	2.25 mm	3 mm	3.75 mm	4.5 mm	5.25 mm	6 mm
Porosity (%)	73.75	62.08	52.03	40.94	31.76	23.92	18.06

Table 1 - Average porosity found in cubic-shaped gyroid structures with different wall thicknesses.

The stress values in both the cubic and bone mimicking, tube-shaped structures were obtained by dividing the applied force by the average area it's applied to. To calculate this area, firstly the volume of the gyroid cubes was calculated, by manufacturing a full 20x20x20 mm cube and weighing it to obtain the filaments' density, which was then used to calculate the gyroid cubes' volume. Afterwards, the volume fraction (1-porosity) was multiplied by the area of a full cubes' face to determine de average area to which the force is applied.

The stress-strain curves were obtained using MATLAB (Figure 8). The code used to plot them as well as the original stress-strain curves (Figure 25) can be found in Annex B.

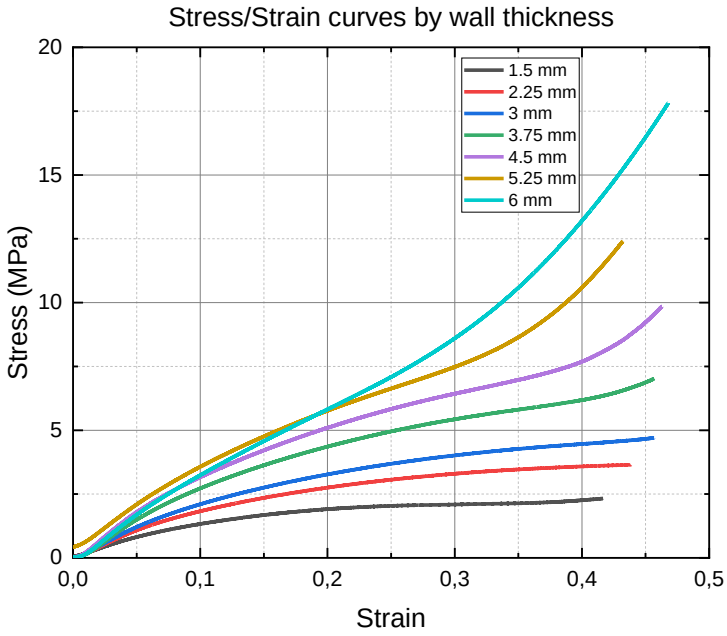

Figure 8 - Average Stress/Strain curves of cubic shaped gyroid structures with increasingly higher wall thickness.

All samples displayed a typical TPU stress-strain curve [35]. The average elasticity modulus for each wall thickness was calculated by taking the initial part of each of the Stress-strain curves that has the most linear like behavior, applying a linear fit on it and extracting its slopes' value (Figure 9). Samples with the same thickness mostly showed very similar stress-strain curves, which is a good indicator that there is little variation in quality between different 3D prints. Samples 2 and 3 from both 1.5 and 4.5 mm thicknesses were the exception, displaying different stress-strain curves compared to what was expected from previous samples, which could be indicative of defects in the 3D printing process. Their curves were thus considered outliers.

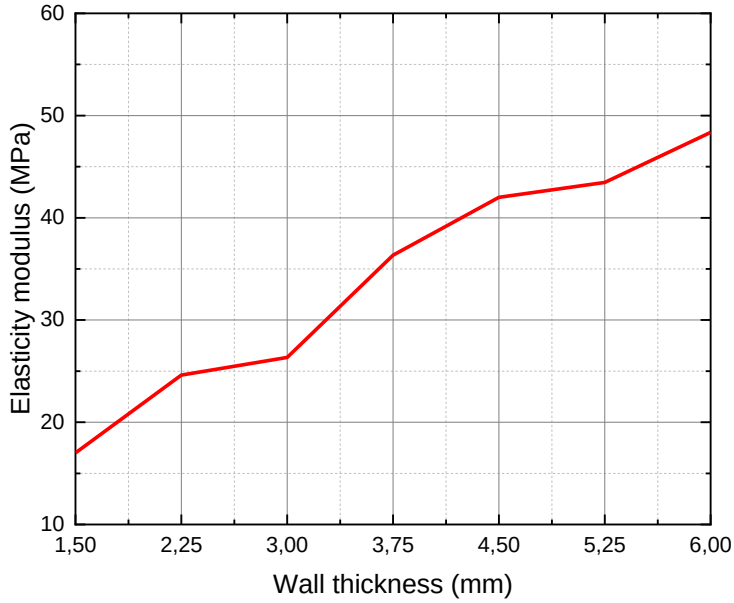

Figure 9 - Evolution of the Elasticity modulus of the cubic structures with increasingly higher wall thickness.

To calculate the values of the structures PR, sets of red dots were painted onto the surface of the structures. To distinguish between different points, these were identified numerically by ordering them from top to bottom, left to right (Figure 10).

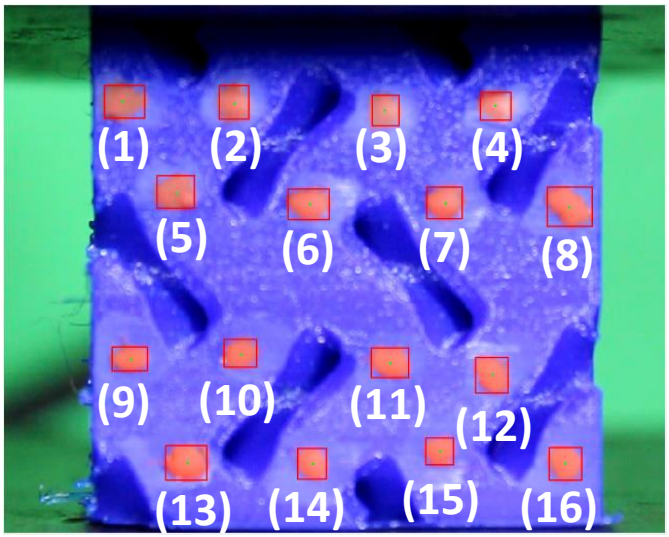

Figure 10 - MATLAB identification of the red dots from sample 1 of the 6 mm wall thickness cubic shaped structure.

Two different pairs of points were evaluated, the first pair being made up of points located far from the center of the face in which they are located, henceforth called exterior points (8 and 9 or equivalent), and the second being made up of points closer to the center of the face, henceforth called interior points (7 and 10 or equivalent). The interior points displayed lower PR values across all samples, which were also more in line with the observed behavior when compared to the exterior points, due to the border effect (Figure 11).

The PR value was shown to increase with increasing thickness (Figure 11). The increase of the wall thickness in the structure appears to constrain the structures capacity to collapse upon itself, therefore decreasing its auxeticity. Only the lowest thickness displayed an auxetic behavior. The two highest wall thickness structures, 5.25 mm and 6 mm, clearly displayed densification beyond 25% strain. The PR also seems to have a tendency to decrease slightly with increasing strain. These results show, however, that tweaking the thickness of the gyroid surface allows for tailor made PRs.

Determining the PR for low strain levels proved to be a challenge, since the adjustment of the structure to the bottom plate inevitably leads to unwanted movement of the painted dots, and for small variations in the distance between drawn points, a variation of a few pixels both in the longitudinal and the transversal direction can lead to drastic changes in the calculated PR value. Most PR-strain curves displayed an erratic behavior for low levels of strain (up to around 10%) (Figures 26-32). The data gathered from the internal points showed an improvement in this aspect, with reduced variation in the PR.

To counter this phenomenon, the gathered data for distance between dots (in both the longitudinal and transversal directions) was loaded into Origin and the curves were subjected to a polynomial fitting to smooth out any noise. The fitted distance curve data was then turned into strain and used to plot smoother PR-Strain curves (Figure 11).

The original MATLAB PR-Strain curves can be found in Annex B (Figures 26-32).

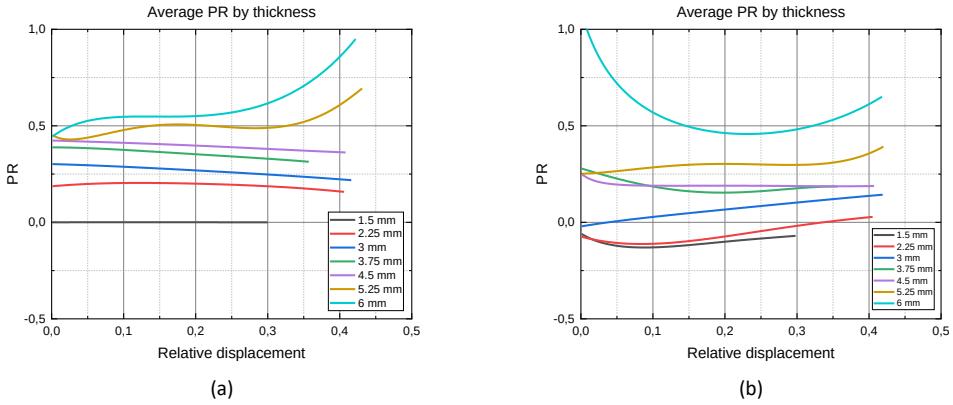

Figure 11 - PR values of cubic shaped gyroid structures with increasingly higher wall thicknesses, after fitting, between internal (a) and external (b) points.

3.3 Bone mimicking structures

A bone mimicking structure was modeled based on the morphology of femoral bone, specifically the shaft of the femur. The cross-section of the femoral shaft has an outer diameter of around 30 mm and an inner diameter of around 20 mm. Trabecular bone is present in the area between a diameter of 20 mm to 25 mm, approximately, and cortical bone is present in the remainder of the area [36]. A thickness gradient from 0.5 mm to 2 mm was introduced in the modeled structure to obtain porosity values like those found in real femoral bone. The results of the compression testing revealed a PR with a high barreling effect being observed (This structure corresponds to the 25 mm inner diameter, with a 0.5-2 mm gradient structure, found in Figure 14 - b)).

To counteract this, the internal diameter was reduced, with the intent of adding an internal stress field, between the new inner diameter and the old inner diameter, which opposes the barreling effect, and the outer diameter was reduced to allow the cells to collapse more easily. The resulting structure displayed a more desirable behavior, with a low yet positive PR.

This also motivated a study of the effect of the inner diameter as well as of the thickness gradient on the structures' PR.

Consequently, 6 structures were printed, subdivided into two different thickness gradients, 0.5-2 mm and 0.5-1.5 mm, and three different inner diameters (Figure 12), 20 mm, 10 mm and 4 mm. All structures were printed with a height of 30 mm. Additionally, a half structure was printed for every model to observe the collapse of the cells during compression (Figure 12).

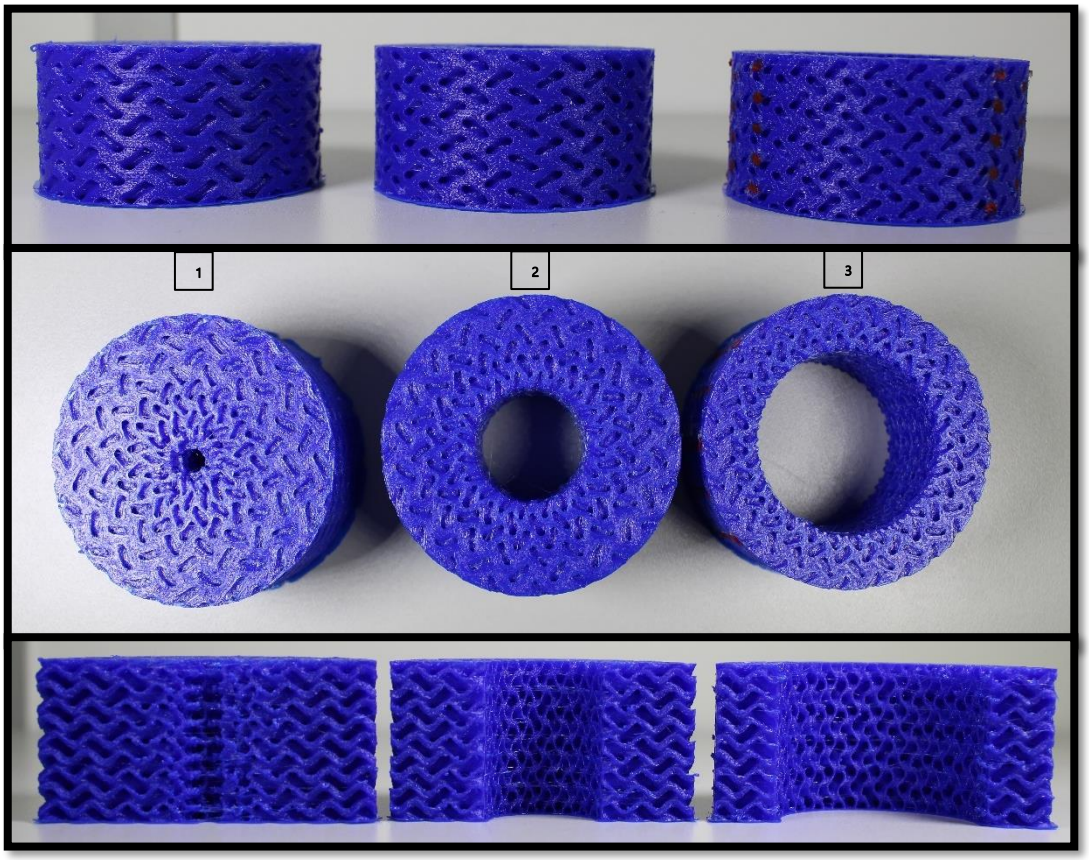

Figure 12 - Bone mimicking structures example, ordered by inner diameter, 4 mm (1), 10 mm (2), 25 mm (3), with a thickness gradient of 0.75-1.5 mm.

However, during the manufacturing of the 0.5-2 mm structures, those with an inner diameter of 4 mm had to have their inner thickness raised, as it was found that the design introduced its own slight thickness gradient, which lowered the inner thickness of the structure. This effect is more pronounced the smaller the inner diameter is, and it was enough to take it under the printers' resolution of 0.4 mm, making printing impossible. The thickness was raised to 0.75 mm as it was the closest value to 0.5 mm which remained inside the printing resolution range.

Another solution would have been to scale up the structure, but this would significantly increase printing time and material expenditure.

The unexpected gradient added by the structures designing was not studied but should be considered in future projects. All 0.5-1.5 mm structures were thus also altered to 0.75-1.5 mm.

Once again, the values of these structures' PR were determined via red varnish dots painted onto the structure, in sets of either 13 or 23 red dots. The different number of dots is imposed by the modelling process of the structure. The PR's calculation was made between dots 10 and 14's positions or equivalent (Figure 13).

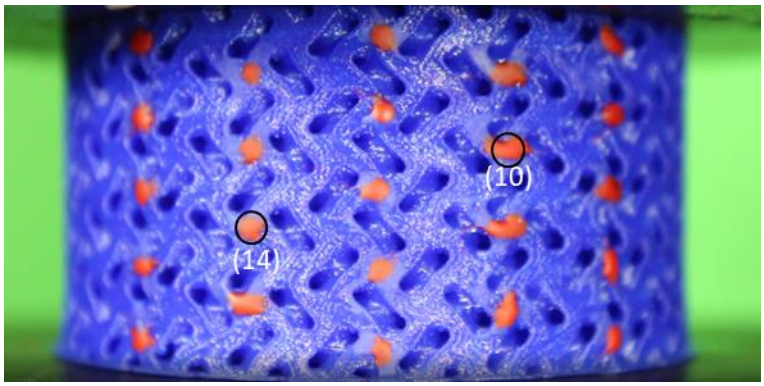

Figure 13 - Bone mimicking sample with 23 red dots painted on it. identification of these dots is made in the same way as in the cubic shaped samples, from top to bottom and from left to right.

The PR of the structures increases with an increase in the inner diameter and with increasing outer wall thickness, in the area corresponding to cortical bone (Figure 14). Once again, for low values of strain it is difficult to accurately determine the PR's value, so the distance between points' curves were once again fitted and smoother PR curves were plotted. The original curves can be found in Annex B (Figure 34-35).

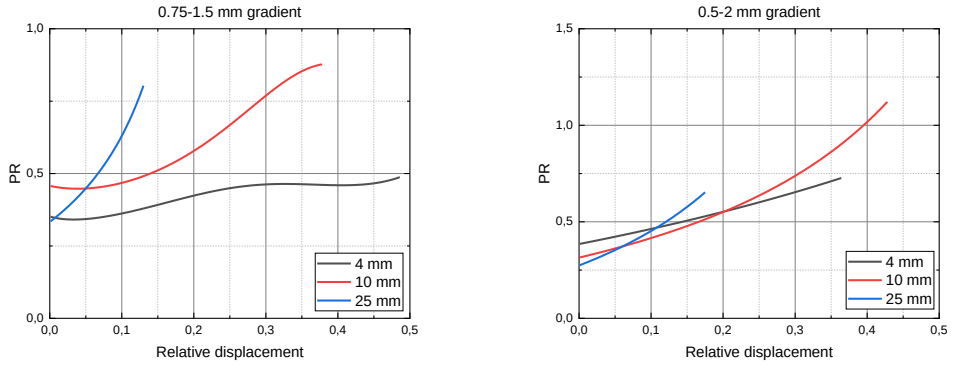

Figure 14 - Effect of the inner diameter and wall thickness gradient in the PR of bone mimicking structures. Note that the 4 mm structure in (b) has a 0.75-2 mm gradient as previously mentioned.

The reduction in the barreling effect with decreasing inner diameter, becomes especially apparent when visualizing only half the structure during deformation (Figure 15). Additionally, adding a thin wall to the inside surface of the structure could further reduce this effect, but that option was not explored in this study.

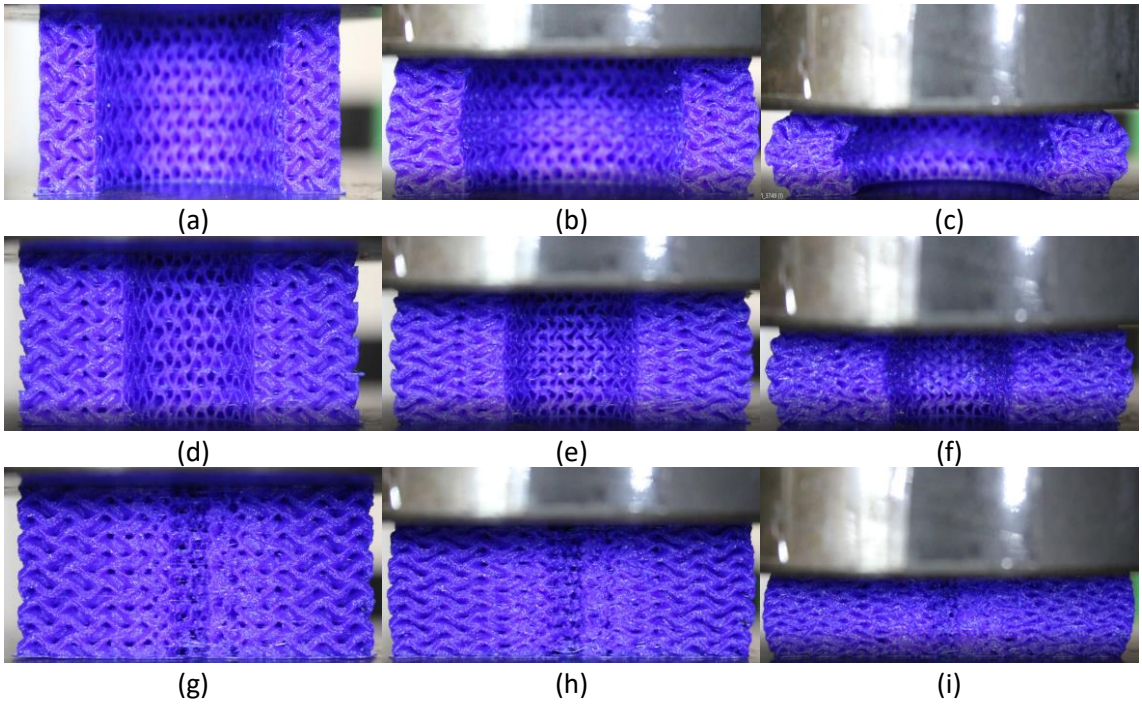

Figure 15 - Visualization of the deformation of bone mimicking structures at the beginning of the compression test (a, d, g), halfway through the compression test (b, e, h) and at the end of the compression test (c, f, i), for structures with a wall thickness gradient of 0.75-1.5 mm with an inner diameter of 4 mm (a, b, c), 10 mm (d, e, f) and 25 mm (g, h, i).

The PR values obtained for all structures, particularly structures with a higher inner diameter, were inflated by a barreling effect on the structure (Figure 16).

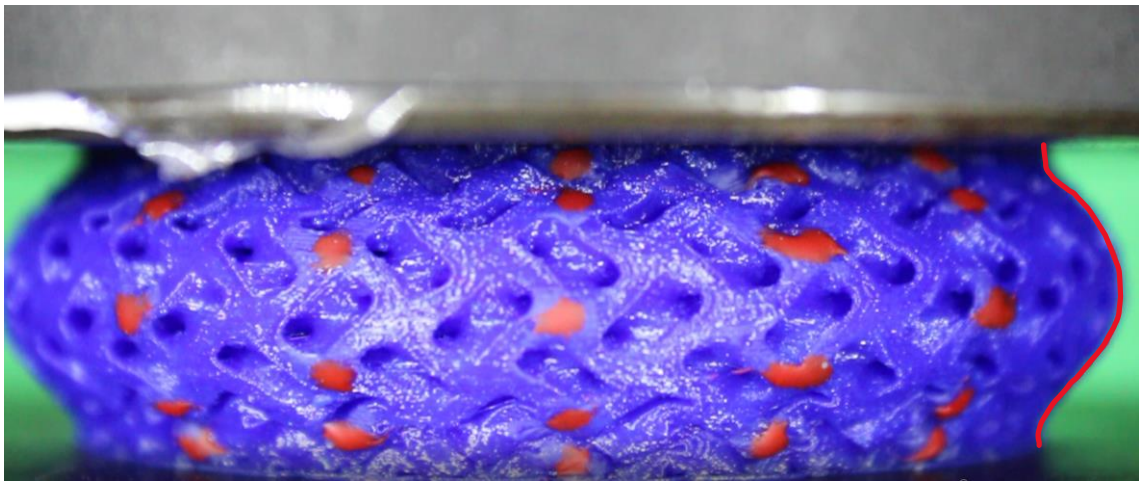

Figure 16 - Barreling effect example, observed in a bone mimicking structure with a 25 mm inner diameter and a wall thickness gradient of 0.5-2 mm.

Despite not achieving the same overall PR as found in real bone, with an average of 0.3 [37], [38], these results point to the possibility that a bone mimicking structure such as this could achieve the same values of PR as the ones found in bone, by adjusting the inner diameter and outer thickness, while simultaneously achieving an auxetic behavior in the area corresponding to trabecular bone, by adjusting the inner thickness of the structure.

4

Conclusions and future prospects

Seven cubic shaped structures based on the gyroid surface, with increasingly higher wall thickness, were produced and characterized to investigate the potential auxetic character of this surface and how the wall thickness impacts its PR. It was found that the PR for structures based on the gyroid surface increases with the increase in wall thickness, and that for low enough wall thicknesses (equal to or lower than 0.5 mm) an auxetic behavior can be obtained. These results show that the gyroid surface can be used to create structures with tailor made PR values.

Furthermore, six distinct bone mimicking structures were modelled after data on the morphology of the cross-section of femoral bone shaft, also based on the gyroid surface, with varying inner diameters and thickness gradients, to study how these two parameters impact the PR of said structures. While an auxetic behavior was not obtained in the produced structures, it was found that reducing their inner diameter and reducing the outside wall thickness reduces the PR value. This hints to the possibility of creating a structure with a tailor-made PR, which mimics real bones' PR values.

To further this study, it would be interesting to model these bone mimicking structures, adjusted with the aim of reducing the barreling effect and thus its PR, to a level similar to the values found in real bone. Additionally, it would be interesting to produce these structures in PLA, and subject them to citotoxicity testing, to determine wether the similarities between the gyroid and trabecular bones' curvatures translate into superior cell growth properties, to perform fatigue testing on these structures, to explore new, more accurate methods of determining the PR, such as the digital image correlation method, and to explore other ways of introducing porosity gradients to gyroid based structures, such as through tweaking of its mathematical equation or via programming software, methods which were already contemplated in this work, but not expanded upon.

BIBLIOGRAPHY

[1] V. H. Carneiro, J. Meireles, and H. Puga, "Auxetic materials - A review," *Materials Science-Poland*, vol. 31, no. 4. pp. 561–571, Oct. 2013. doi: 10.2478/s13536-013-0140-6.

[2] J. H. Roh, C. B. Giller, P. H. Mott, and C. M. Roland, "Failure of classical elasticity in auxetic foams ARTICLES YOU MAY BE INTERESTED IN Failure of classical elasticity in auxetic foams," *AIP Advances*, vol. 3, p. 42126, 2013, doi: 10.1063/1.4802925.

[3] R. Lakes, "Foam structures with a negative poisson's ratio," *Science*, vol. 235, no. 4792, pp. 1038–1040, Feb. 1987, doi: 10.1126/science.235.4792.1038.

[4] S. J. Kalita, "Rapid prototyping in biomedical engineering: Structural intricacies of biological materials," in *Biointegration of Medical Implant Materials: Science and Design*, Elsevier Ltd., 2010, pp. 349–397. doi: 10.1533/9781845699802.3.349.

[5] A. Di Luca, A. Longoni, G. Criscenti, C. Mota, C. Van Blitterswijk, and L. Moroni, "Toward mimicking the bone structure: Design of novel hierarchical scaffolds with a tailored radial porosity gradient," *Biofabrication*, vol. 8, no. 4, Oct. 2016, doi: 10.1088/1758-5090/8/4/045007.

[6] J. L. Williams and J. L. Lewis, "Properties and an anisotropic model of cancellous bone from the proximal tibial epiphysis," *Journal of Biomechanical Engineering*, vol. 104, no. 1, pp. 50–56, 1982, doi: 10.1115/1.3138303.

[7] N. Ghavidelnia, M. Bodaghi, and R. Hedayati, "Femur Auxetic Meta-Implants with Tuned Micromotion Distribution," *Materials (Basel, Switzerland)*, vol. 14, no. 1, pp. 1–30, Jan. 2020, doi: 10.3390/MA14010114.

[8] H. M. A. Kolken, S. Janbaz, S. M. A. Leeflang, K. Lietaert, H. H. Weinans, and A. A. Zadpoor, "Rationally designed meta-implants: A combination of auxetic and conventional meta-biomaterials," *Materials Horizons*, vol. 5, no. 1, pp. 28–35, Jan. 2018, doi: 10.1039/c7mh00699c.

[9] H. M. A. Kolken *et al.*, "Mechanical performance of auxetic meta-biomaterials," *Journal of the Mechanical Behavior of Biomedical Materials*, vol. 104, p. 103658, Apr. 2020, doi: 10.1016/j.jmbbm.2020.103658.

[10] C. N. Kelly *et al.*, "Functional repair of critically sized femoral defects treated with bioinspired titanium gyroid-sheet scaffolds," *Journal of the Mechanical Behavior of Biomedical Materials*, vol. 116, p. 104380, Apr. 2021, doi: 10.1016/j.jmbbm.2021.104380.

[11] L. Mizzi *et al.*, "Mechanical metamaterials with star-shaped pores exhibiting negative and zero Poisson's ratio," *Materials and Design*, vol. 146, pp. 28–37, May 2018, doi: 10.1016/j.matdes.2018.02.051.

[12] X. T. Wang, X. W. Li, and L. Ma, "Interlocking assembled 3D auxetic cellular structures," *Materials and Design*, vol. 99, pp. 467–476, Jun. 2016, doi: 10.1016/j.matdes.2016.03.088.

[13] L. Wu, B. Li, and J. Zhou, "Isotropic Negative Thermal Expansion Metamaterials," *ACS Applied Materials and Interfaces*, vol. 8, no. 27, pp. 17721–17727, Jul. 2016, doi: 10.1021/acsami.6b05717.

[14] K. Wei, Y. Peng, Z. Qu, Y. Pei, and D. Fang, "A cellular metastructure incorporating coupled negative thermal expansion and negative Poisson's ratio," *International Journal of Solids and Structures*, vol. 150, pp. 255–267, Oct. 2018, doi: 10.1016/j.ijsolstr.2018.06.018.

[15] X. Li, L. Gao, W. Zhou, Y. Wang, and Y. Lu, "Novel 2D metamaterials with negative Poisson's ratio and negative thermal expansion," *Extreme Mechanics Letters*, vol. 30, p. 100498, Jul. 2019, doi: 10.1016/j.eml.2019.100498.

[16] J. N. Grima and R. Caruana-Gauci, "Mechanical metamaterials: Materials that push back," *Nature Materials*, vol. 11, no. 7. Nature Publishing Group, pp. 565–566, Jun. 21, 2012. doi: 10.1038/nmat3364.

[17] M. Fu, Y. Chen, W. Zhang, and B. Zheng, "Experimental and numerical analysis of a novel three-dimensional auxetic metamaterial," *physica status solidi (b)*, vol. 253, no. 8, pp. 1565–1575, Aug. 2016, doi: 10.1002/pssb.201552769.

[18] A. Love, "A treatise on the mathematical theory of elasticity."

[19] H. Kimizuka, H. Kaburaki, and Y. Kogure, "Mechanism for negative poisson ratios over the α-β transition of cristobalite, SiO2: a molecular-dynamics study," *Physical Review Letters*, vol. 84, no. 24, pp. 5548–5551, Jun. 2000, doi: 10.1103/PhysRevLett.84.5548.

[20] J. N. Grima, R. Gatt, A. Alderson, and K. E. Evans, "On the origin of auxetic behaviour in the silicate α-cristobalite," *Journal of Materials Chemistry*, vol. 15, no. 37, pp. 4003–4005, Oct. 2005, doi: 10.1039/b508098c.

[21] A. Alderson and K. E. Evans, "Molecular Origin of Auxetic Behavior in Tetrahedral Framework Silicates," *Physical Review Letters*, vol. 89, no. 22, 2002, doi: 10.1103/PhysRevLett.89.225503.

[22] J. N. Grima and K. E. Evans, "Auxetic behavior from rotating triangles," *Journal of Materials Science*, vol. 41, no. 10, pp. 3193–3196, May 2006, doi: 10.1007/s10853-006-6339-8.

[23] P. V. Pikhitsa, "Regular network of contacting cylinders with implications for materials with negative poisson ratios," *Physical Review Letters*, vol. 93, no. 1, p. 015505, Jul. 2004, doi: 10.1103/PhysRevLett.93.015505.

[24] L. Gu, Q. Xu, D. Zheng, H. Zou, Z. Liu, and Z. Du, "Analysis of the mechanical properties of double arrowhead auxetic metamaterials under tension," *Textile Research Journal*, vol. 90, no. 21–22, pp. 2411–2427, Nov. 2020, doi: 10.1177/0040517520924850.

[25] X. T. Wang, B. Wang, X. W. Li, and L. Ma, "Mechanical properties of 3D re-entrant auxetic cellular structures," *International Journal of Mechanical Sciences*, vol. 131–132, pp. 396–407, Oct. 2017, doi: 10.1016/j.ijmecsci.2017.05.048.

[26] Y. Wang *et al.*, "Numerical and experimental studies on compressive behavior of Gyroid lattice cylindrical shells," *Materials and Design*, vol. 186, p. 108340, Jan. 2020, doi: 10.1016/j.matdes.2019.108340.

[27] A. A. Zadpoor, "Meta-biomaterials," *Biomaterials science*, vol. 8, no. 1, pp. 18–38, Jan. 2019, doi: 10.1039/C9BM01247H.

[28] K. MONKOVA, P. MONKA, I. ZETKOVA, P. HANZL, and D. MANDULAK, "Three Approaches to the Gyroid Structure Modelling as a Base of Lightweight Component Produced by Additive Technology," *DEStech Transactions on Computer Science and Engineering*, no. cmsam, Dec. 2017, doi: 10.12783/dtcse/cmsam2017/16361.

[29] J. C. Najmon, S. Raeisi, and A. Tovar, "Review of additive manufacturing technologies and applications in the aerospace industry," in *Additive Manufacturing for the Aerospace Industry*, Elsevier Inc., 2019, pp. 7–31. doi: 10.1016/B978-0-12-814062-8.00002-9.

[30] J. Zhang, G. Lu, Z. Wang, D. Ruan, A. Alomarah, and Y. Durandet, "Large deformation of an auxetic structure in tension: Experiments and finite element analysis," *Composite Structures*, vol. 184, pp. 92–101, Jan. 2018, doi: 10.1016/j.compstruct.2017.09.076.

[31] L. Wang *et al.*, "Latitude-and-longitude-inspired three-dimensional auxetic metamaterials," *Extreme Mechanics Letters*, vol. 42, p. 101142, Jan. 2021, doi: 10.1016/j.eml.2020.101142.

[32] H. M. A. Kolken and A. A. Zadpoor, "Auxetic mechanical metamaterials," *RSC Advances*, vol. 7, no. 9. Royal Society of Chemistry, pp. 5111–5129, Jan. 17, 2017. doi: 10.1039/c6ra27333e.

[33] X. Ren, R. Das, P. Tran, T. D. Ngo, and Y. M. Xie, "Auxetic metamaterials and structures: A review," *Smart Materials and Structures*, vol. 27, no. 2. Institute of Physics Publishing, p. 023001, Jan. 24, 2018. doi: 10.1088/1361-665X/aaa61c.

[34] G. Catatão, "Additive Manufacturing and Characterization of Three-dimensional Anepectic Structures," Lisbon, 2022.

[35] H. J. Qi and M. C. Boyce, "Stress-Strain Behavior of Thermoplastic Polyurethane".

[36] D. A. Nelson, D. A. Barondess, S. L. Hendrix, and T. J. Beck, "Cross-sectional geometry, bone strength, and bone mass in the proximal femur in black and white postmenopausal women," *Journal of bone and mineral research : the official journal of the American Society for Bone and Mineral Research*, vol. 15, no. 10, pp. 1992–1997, 2000, doi: 10.1359/JBMR.2000.15.10.1992.

[37] D. Christian Wirtz *et al.*, "Critical evaluation of known bone material properties to realize anisotropic FE-simulation of the proximal femur," *Journal of Biomechanics*, vol. 33, pp. 1325–1330, 2000.

[38] R. M. Pidaparti and A. Vogt, "Experimental investigation of Poisson's ratio as a damage parameter for bone fatigue," *Journal of Biomedical Materials Research*, vol. 59, no. 2, pp. 282–287, 2002, doi: 10.1002/JBM.1243.

A

ANNEX A - DESIGN

A.1 Gyroid generation in MATLAB

The gyroid surface was generated using the following code:

```
clear all
close all
clc


%dimensions of the generated surface
%gyroid cells repeat after every Pi

x_period = 2;
y_period = 2;
z_period = 2;

%3.15 was used instead of the real value of Pi because the latter caused
%problems when trying to generate the cylindrical structures

[x,y,z] = meshgrid(-x_period*3.15:0.1:x_period*3.15, -
y_period*3.15:0.1:y_period*3.15, -z_period*3.15:0.1:z_period*3.15);

%gyroid function

f = sin(x).*cos(y) + sin(y).*cos(z) + sin(z).*cos(x);

%generates the 3D surface and displays it

figure(1)
isosurface(x,y,z,f)
axis equal
xlabel('X')
ylabel('Y')
zlabel('Z')

%saves the surface in an stl file

fv = isosurface(x,y,z,f);

  stlwrite('Gyroid3.stl',fv)
```

The MATLAB version used in this study (R2019a) does not have an integrated stlwrite function. The function utilized was extracted from https://old.reddit.com/r/3Dprinting/comments/858ypy/modeling_a_gyroid/.

A.2 Cubic structure design

All cubic structures were based on a 4x4x4 cell gyroid surface generated in MATLAB. These were then given a thickness from 0.5 mm to 2 mm, in steps of 0.25 mm, using the solidify tool in the open-source Blender software. They were then trimmed using a cube with 12.3 mm side length and a Boolean modifier, to obtain a smooth surface for mechanical testing (Figure 17).

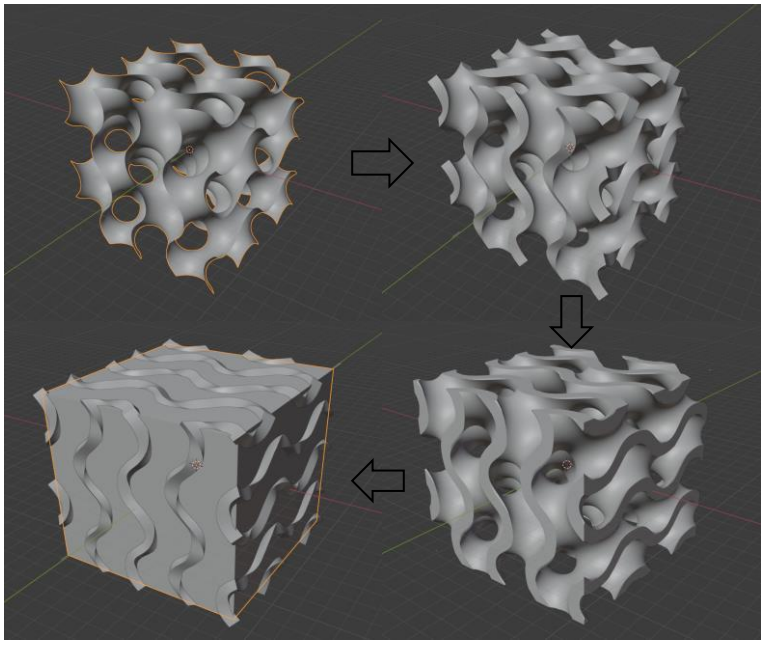

Figure 17 - Schematic of the modelling of a cubic shaped gyroid structure with a wall thickness of 0.75 mm.

Finally they were exported in .stl format, which can then be recognized by Cura, the slicing software used for the FDM 3D printing. In Cura, the dimensions of the cubes were scaled up 300%, resulting in cubes with a side of 36.9 mm. The purpose of this is to obtain a better print resolution and reduce the impact of any possible printing defects.

A.3 Cylindrical structure design

To model the bone mimicking structures, firstly a gyroid surface with the appropriate length was generated through MATLAB (26 mm for a 4 mm diameter structure, 20 mm for a 10 mm inner diameter structure and 10 mm for a 25 mm inner diameter structure), and a multiple of π for width, since the gyroid surface repeats itself every π (Figure 18).

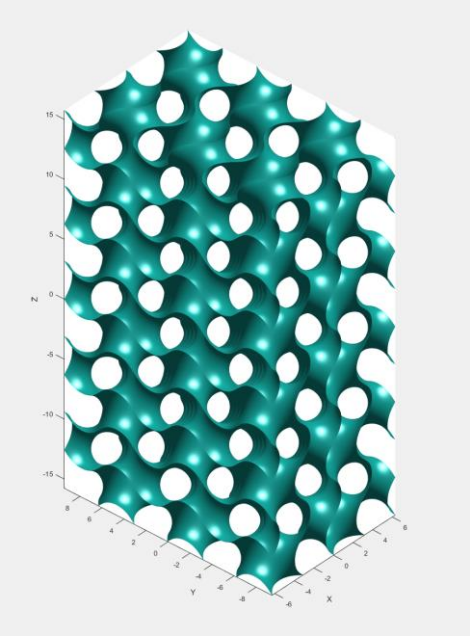

Figure 18 - Gyroid surface generated for modelling a 10 mm inner diameter bone mimicking structure.

Afterwards, this surface was loaded into the Blender software. In Blender, this surface is turned into a mesh, and the vertexes in the mesh can then be placed in a vertex group, which will only be used to refer to these vertexes later (Figure 19). Then, using the weight paint tool, the vertexes can be assigned values that will determine how much any given modifier will be affecting them, relative to the selected value. This means that, for example, when applying a thickness of 1 mm to the vertex group, vertexes with a weight value of 0.5 will only receive a thickness of 0.5 mm.

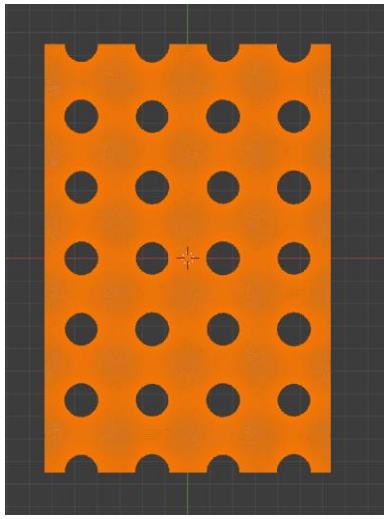

Figure 19 - Vertex group generated in Blender for the gyroid model.

Using the linear gradient weight paint tool, a weight gradient is applied roughly in the middle of the structure, along the y axis, with the appropriate gradient (Figure 20). To obtain a 0.5-2 mm gradient for example, a 0.25-1 weight gradient would be used.

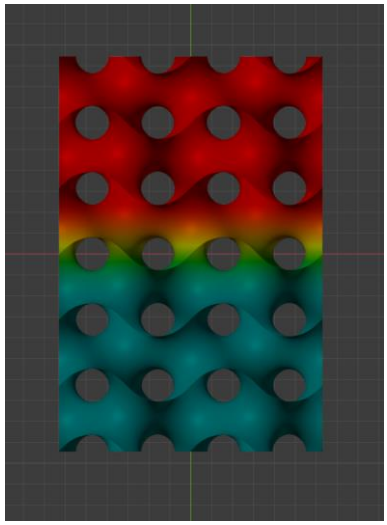

Figure 20 - Weight profile applied to the vertexes in the model. The red color represents 100% weight, while blue represents 25% weight. The transition happens only in the middle of the structure.

Then, when applying a thickness to the surface, using the solidify modifier, the result is an abrupt wall thickness gradient near the middle of the structure. The resulting structure needs to be trimmed to obtain smooth surfaces for mechanical testing, except in the x direction, since that would prevent proper joining of the structure array later (Figure 21). To trim the structure, a rectangular parallelepiped was used with a boolean modifier.

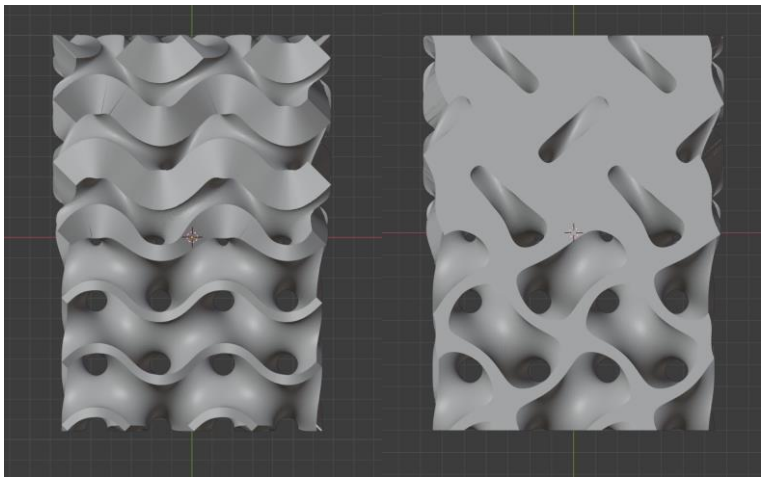

(a) (b)

Figure 21 - Structure before (a) and after trimming (b).

Finally, to transform this structure into a tube-shaped form, it needs to be multiplied and made into an array using the array modifier, and then it can be made to adopt a circular shape by applying a curve modifier on a Nurbs circle (Figure 22). It's important to note that the curve modifier will cause inadvertent thickness gradient, which should be taken into account. The Nurbs circle needs to have the average diameter between the desired inner and outer diameter of the final structure since the elements of the array will be centered on it.

To obtain a perfect fit between array elements, a constant offset of 12.57 mm was applied on the array modifiers' properties menu. The number of elements in the array depends on the structures' inner diameter. The Nurbs circle diameter typically needs to be tweaked to allow for the first and last elements of the array to perfectly fit onto each other.

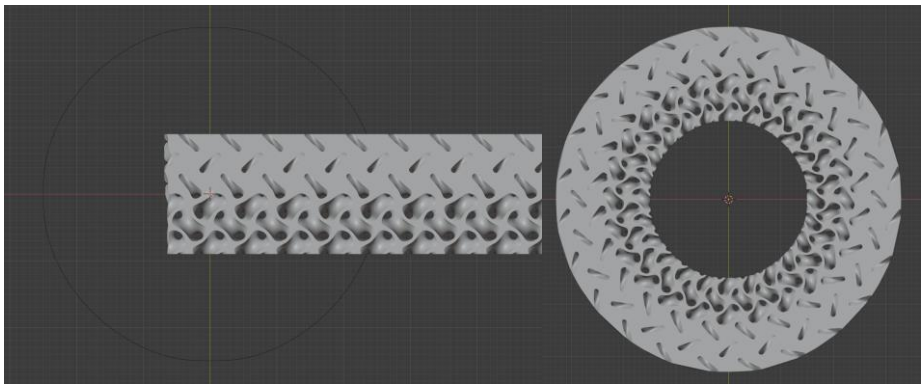

(a) (b)

Figure 22 - Structure after being made into an array (a), and after being applied the curve modifier to the Nurbs circle (b).

Sometimes, after the modelling process is done, black artifacts will appear on the structure. These correspond to problems in the generated mesh of the structure (Figure 23). Applying a decimate modifier, which reduces the number of vertexes to an arbitrary percentage of the original amount, and/or a weld modifier, which fuses mesh lines closer to each other than a certain threshold distance, seems to solve this problem for the most part, although there are other tools available in Blender to clean up meshes.

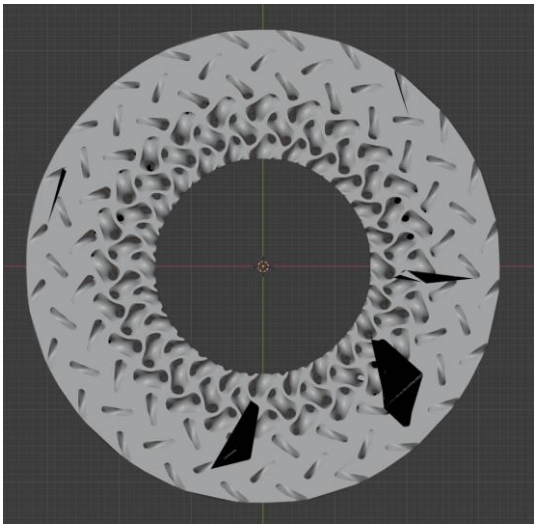

Figure 23 - Black artifacts in the bone mimicking structure after modeling.

After this, the structure is exported in .stl format to Cura, where It can be scaled up or down to the exact desired dimensions, and it's ready to be printed.

A.4 Printing parameters

The main printing parameters used to print all structures can be found below:

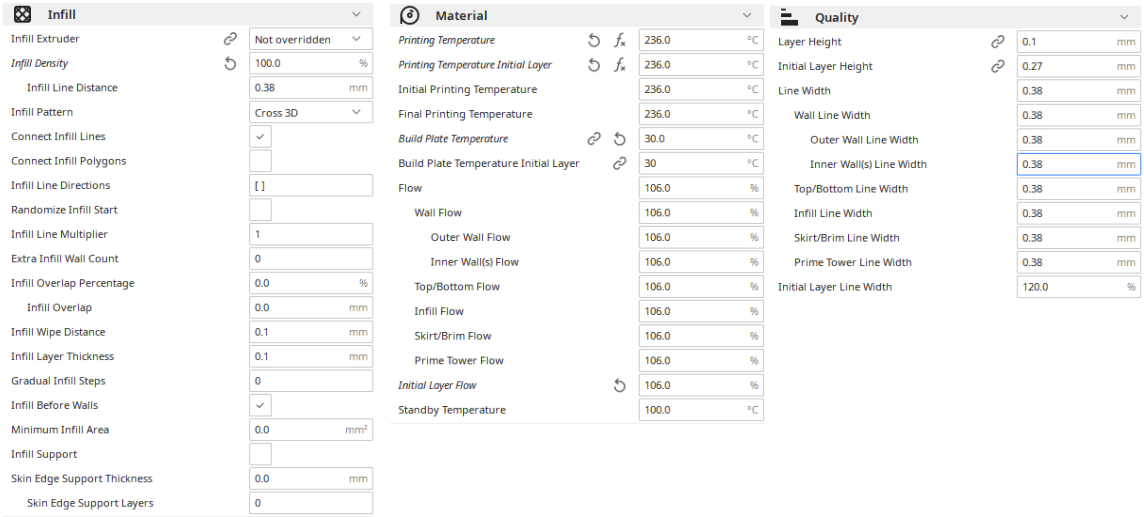

Figure 24 - Main parameters used for the printing of the structures.

B

ANNEX B -MECHANICAL CHARACTERIZATION

B.1 MATLAB code used for mechanical characterization

Mechanical characterization and PR determination was performed using the following code:

```
clear all
close all

%%data analysis
%%open data file obtained from mechanical tests

fig = 1;

fid=fopen('Amostra 1 0.5.txt');
tline = fgetl(fid);
tlines = cell(0,1);
num_line = 0;
data = cell(0,4);

%%input actual volume of the sample

prompt_1 = {'Volume (mm^3):'};
dlgtitle_1 = 'Dados';
dims = [1 35];
definput_1 = {'12566'};
answer_1 = inputdlg(prompt_1,dlgtitle_1,dims,definput_1);
volume = str2double(answer_1{1});

time_data = [];
force_data = [];
stroke_data = [];
extension_z_data = [];
tension_data = [];

%%input the stroke value at which force starts being applied to the sample
```

```
prompt_2 = {'Conpensated stroke (mm):'};
dlgtitle_2 = 'Shift data';
definput_2 = {'2.92'};
answer_2 = inputdlg(prompt_2,dlgtitle_2,dims,definput_2);
stroke_shift = str2double(answer_2{1});

while ischar(tline)
    num_line = num_line + 1;
    if num_line == 11
        tlines{end+1,1} = tline;
        final = split(tlines{end});
        dist_x = str2double(replace(final{5} ,",",".")); %dimension of the
sample in x
        dist_y = str2double(replace(final{6} ,",",".")); %dimension of the
sample in y
        dist_z = str2double(replace(final{7} ,",",".")); %dimension of the
sample in z
        volume_ap = dist_x * dist_y * dist_z; %calculate apparent volume
        area_ap = dist_x * dist_y; %calculate apparent area
        area = (volume / volume_ap) * area_ap; %calculate area where force
is applied
        compensated_strain = stroke_shift./dist_z; %turn compensated stroke
into strain
    elseif num_line > 21
        tlines{end+1,1} = tline;
        final = split(tlines{end});
        real_time = str2double(replace(final{1} ,",",".")); %test time data
        force = str2double(replace(final{2} ,",",".")); %test force data
        stroke = str2double(replace(final{3} ,",",".")) - stroke_shift;
%compensated test stroke data

        %%save data only from beyond the compensated stroke

        if stroke >= 0
            time_data(end + 1) = real_time; %seconds
            force_data(end + 1) = force * 1000; %Newton
            stroke_data(end + 1) = stroke; %mm
            extension_z_data(end + 1) = stroke/dist_z; %turn stroke to
strain
            tension_data(end + 1) = (force * 10^3)/(area * 10^-6); %Pa
(N/m^2)
        end
    end
    tline = fgetl(fid);
end
fclose(fid);

% stress-strain and stress-stroke graphics

figure(fig)
plot(extension_z_data, tension_data)
title('Stress vs Strain')
xlabel('Strain (%)')
ylabel('Stress (Pa)')
fig = fig +1;

figure(fig)
plot(stroke_data, tension_data)
```

```
title('Stress vs stroke')
xlabel('Stroke (mm)')
ylabel('Stress (Pa)')
fig = fig +1;

%%open video

vid=VideoReader('E:\Tese\Caracterização\Gyroid TPU Ultimaker 0.5\Amostra
1\Amostra 1 0.5.MOV');

%%input tests planned maximum strain and desired step
%%the step will determine the amount of points generated for the graphics
%%the true maximum strain will be calculated via the compensated strain

prompt_3 = {'Maximum:','Step:'};
dlgtitle_3 = 'Video strain';
definput_3 = {'0.5','0.001'};
answer_3 = inputdlg(prompt_3,dlgtitle_3,dims,definput_3);
maximum_extension = str2double(answer_3{1})-compensated_strain;
step = str2double(answer_3{2});

extension_video = 0 : step : maximum_extension;

%%input time between the start of the video and the start of the test

prompt_4 = {'Extra time (s):'};
dlgtitle_4 = 'Extra time';
definput_4 = {'3'};
answer_4 = inputdlg(prompt_4,dlgtitle_4,dims,definput_4);
extra_time = str2double(answer_4{1});

%%find desired strain points from the raw data and respective time data

for s = 1:length(extension_video)
    index_resolution = 1e-06;
    index = find(abs(extension_z_data - extension_video(s)) <
index_resolution);
    if isempty(index)
        while isempty(index)
            index_resolution = index_resolution + 1e-06;
            index = find(abs(extension_z_data - extension_video(s)) <
index_resolution);
        end
    elseif length(index) > 3
        while length(index) > 3
            index_resolution = index_resolution - 1e-06;
            index = find(abs(extension_z_data - extension_video(s)) <
index_resolution);
        end
    end

      vid.CurrentTime = time_data(index(ceil(length(index)./2))) +
extra_time;
      time_video(s) = time_data(index(ceil(length(index)./2)));
    ImS = readFrame(vid);
```

```
    if s == 1
        pergunta1 = questdlg('Já sabe os dados iniciais?','Pergunta 1');
        if strcmp(pergunta1,'No')
            figure(fig)
            imshow(ImS)
            return
        end

%%input known real distance vs distance in pixels for unit conversion

        prompt_5 = {'Distancia (mm):','Numero de pixeis:'};
        dlgtitle_5 = 'Dados';
        definput_5 = {'36.3','410'};
        answer_5 = inputdlg(prompt_5,dlgtitle_5,dims,definput_5);
        dist = str2double(answer_5{1});
        pixeis = str2double(answer_5{2});
        Um_Pixel_cm = dist / pixeis;

        prompt_6 = {'Minimum x:','Maximum x:','Minimum y:','Maximum y:'};
        dlgtitle_6 = 'Crop image';
        definput_6 = {'410' , '870' , '200' , '620'};
        answer_6 = inputdlg(prompt_6,dlgtitle_6,dims,definput_6);
        Minimum_x = str2double(answer_6{1});
        Maximum_x = str2double(answer_6{2});
        Minimum_y = str2double(answer_6{3});
        Maximum_y = str2double(answer_6{4});
    end

    ImS = ImS(Minimum_y:Maximum_y, Minimum_x:Maximum_x, :);

%%identify red dots via RGB indexes and their central points

    I_Red = ImS(:,:,1);
    I_Green = ImS(:,:,2);
    I_Blue = ImS(:,:,3);

    mask = ((I_Red >= 175 & I_Green <= 210 & I_Blue <= 220) & (abs(I_Red -
I_Green) > 60) & (abs(I_Red - I_Blue) > 60)) | (I_Red >= 120 & I_Green <=
100 & I_Blue <= 100) | (I_Red >= 95 & I_Green <= 40 & I_Blue <= 40) |
(I_Red >= 59 & I_Green <= 40 & I_Blue <= 40);
    mask = imfill(mask, 'holes');

    positions_centroid = regionprops(mask,'centroid');

    positions = regionprops(mask,'BoundingBox');

%%discard dots smaller than desired threshold

    for i = length(positions):-1:1
        if  positions(i).BoundingBox(3) * positions(i).BoundingBox(4) < 10
            positions_centroid(i) = [];
            positions(i) = [];
        end
    end
```

```
    num_shape = length(positions);

%% stop tracking if the number of dots either exceeds or is less than
desired and extract results
%% display point in which the number of points changed for possible
optimization

    if num_shape ~= 16
        figure(fig)
        subplot(1,2,1), imshow(mask);
        title(num2str(num_shape));
        subplot(1,2,2), imshow(ImS);
        for k = 1 : length(positions)
            all_positions = positions(k).BoundingBox;
            rectangle('Position',
[round(positions_centroid(k).Centroid(1)),round(positions_centroid(k).Centr
oid(2)),1,1],'EdgeColor','g','LineWidth',1)
            rectangle('Position',
[all_positions(1),all_positions(2),all_positions(3),all_positions(4)],'Edge
Color','r','LineWidth',1 )
        end
        title(['extension',num2str(extension_video(s))]);
        fig = fig + 1;
break
    end

%%sort dots by vertical position and then by horizontal position

    T = struct2table(positions_centroid); % convert the struct array to a
table
    Table = T.Centroid;
    Table = sortrows(Table,2); % sort the table by second column
    Table_Linha_1 = sortrows(Table(1:4,:),1);
    Table_Linha_2 = sortrows(Table(5:8,:),1);
    Table_Linha_3 = sortrows(Table(9:12,:),1);
    Table_Linha_4 = sortrows(Table(13:16,:),1);

%%calculate distance between desired points
%%turn distance into strain

    distance_8_9 = (Table_Linha_2(4,1)-Table_Linha_3(1,1)).*(Um_Pixel_cm);
    all_distance_8_9(s) = distance_8_9;
    extension_8_9(s) = (distance_8_9-
all_distance_8_9(1))/all_distance_8_9(1);

    distance_xy = mean([distance_8_9]);

    all_distance_xy(s) = distance_xy;

    extension_xy(s) = (distance_xy - all_distance_xy(1)) ./
all_distance_xy(1);

    distance_8_9 = (Table_Linha_2(4,2)-Table_Linha_3(1,2)).*(Um_Pixel_cm);
    all_distance_8_9(s) = distance_8_9;
    extension_8_9(s) = (distance_8_9-
all_distance_8_9(1))/all_distance_8_9(1);
```

```
    distance_z = mean([distance_8_9]);

    all_distance_z(s) = distance_z;

    extension_z(s) = (distance_z - all_distance_z(1)) ./ all_distance_z(1);

    extension_z_maquina(s) = - extension_z_data(index(1));

end

%%calculate the PR

Poisson = - extension_xy(2:end) ./ extension_z(2:end);
for i = 1:length(Poisson)
    if Poisson(i) == -Inf || Poisson(i) == 0 || Poisson(i) == Inf ||
isnan(Poisson(i))
        Poisson(i) = 0;
    elseif Poisson(i) >= 2 || Poisson(i) <= -2
        Poisson(i) = 2;
    end
end

%%plot desired graphics
%%distance vs time
%%strain vs time
%%PR vs time

figure(fig)
plot(time_video(1:s-1),all_distance_z)
hold on
plot(time_video(1:s-1),all_distance_xy)
hold off
title('Distance between points vs Strain')
xlabel('Strain')
ylabel('Distance (cm)')
legend('z','xy')
fig = fig + 1;

figure(fig)
plot(time_video(1:s-1),extension_xy)
hold on
plot(time_video(1:s-1),extension_z)
title('Strain between points vs overall strain')
xlabel('Overall Strain')
ylabel('Strain between points')
legend('xy','z')
fig = fig + 1;

figure(fig)
plot(time_video(2:s-1),Poisson)
title('Poisson ratio vs Strain')
xlabel('Strain')
ylabel('Poisson ratio')
fig = fig + 1;
```

```
%%input choice to save data

question_save = questdlg('Pretende guardar dados?','Pergunta 2');
if strcmp(question_save,'No')
    return
end

%%save graphic data in excel for treatment

Final_data_1 = num2cell([time_data.' force_data.' stroke_data.'
extension_z_data.' tension_data.']);
header_1 = {'Time (s)','Force (N)','Stroke (mm)','Strain', 'Stress (Pa)'};
output_matrix_1=[header_1; Final_data_1];

xlswrite('Amostra 1 0.5.xls',output_matrix_1,'Stress vs strain','A1');

Final_data_2 = num2cell([dist_x dist_y dist_z area volume]);
header_2 = {'Distance x (mm)','Distance y (mm)','Distance z (mm)','Area',
'Sample volume'};
output_matrix_2=[header_2; Final_data_2];

xlswrite('Amostra 1 0.5.xls',output_matrix_2,'Stress vs strain','F1');

Final_data_3 = num2cell([time_video(1:s-1).' extension_video(1:s-1).'
all_distance_xy.' all_distance_z.' extension_xy.' extension_z.']);
header_3 = {'Time (s)','Strain','Distance between points in xy (cm)',
'Distance between points in z (cm)', 'Strain between points xy' ,'Strain
between points z'};
output_matrix_3 = [header_3; Final_data_3];

xlswrite('Amostra 1 0.5.xls',output_matrix_3,'Poisson','A1');

Final_data_4 = num2cell([time_video(2:s-1).' extension_video(2:s-1).'
Poisson.']);
header_4 = {'Time (s)', 'Strain', 'Poisson'};
output_matrix_4=[header_4; Final_data_4];

xlswrite('Amostra 1 0.5.xls',output_matrix_4,'Poisson','H1');
```

B.2 Stress / Relative displacement results

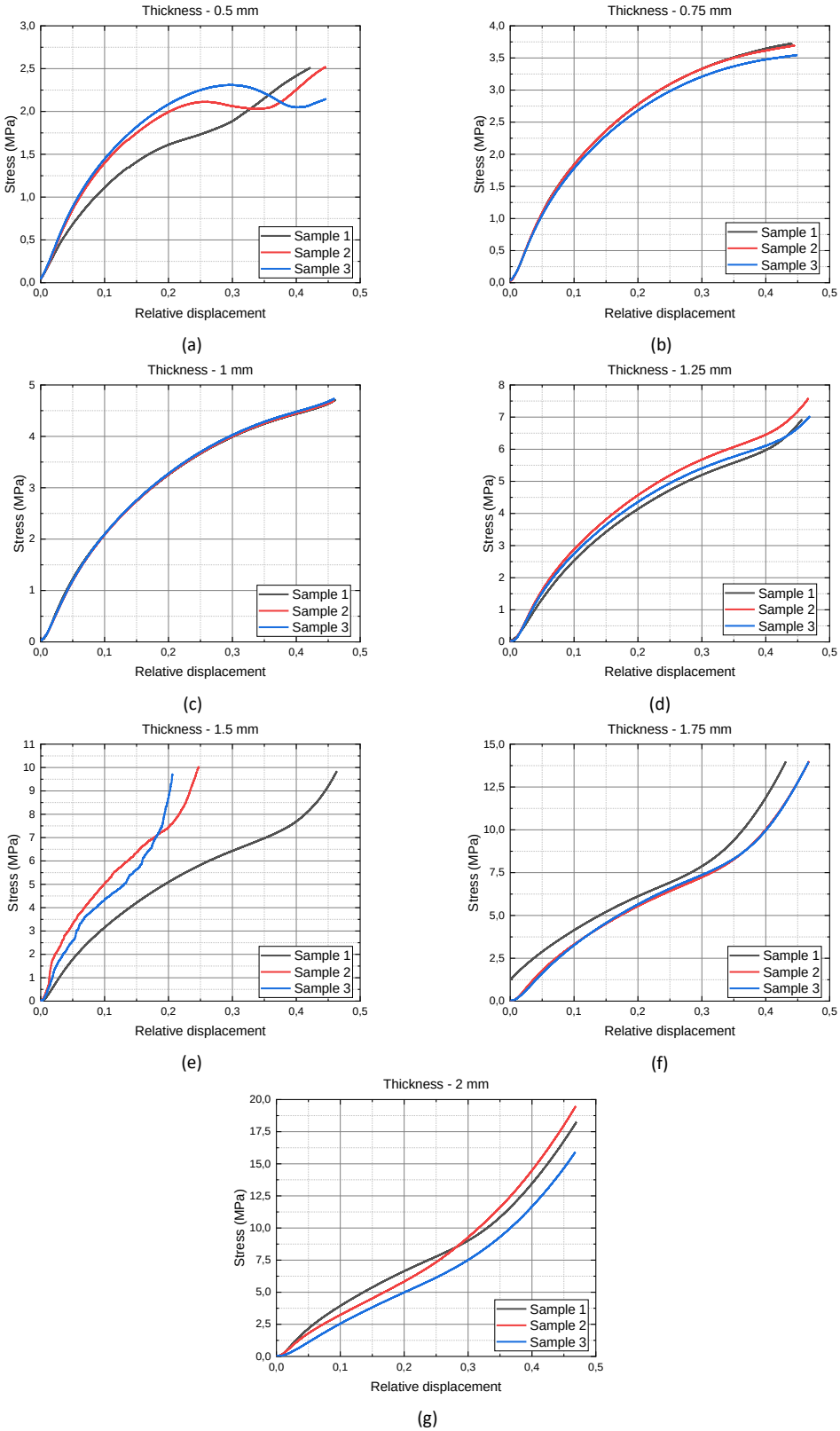

Figure 25 - Stress - Relative displacement curves of gyroid based, cubic-shaped structures, with wall thicknesses varying from 0.5 mm to 2 mm (a-g).

B.3 PR / Relative displacement results

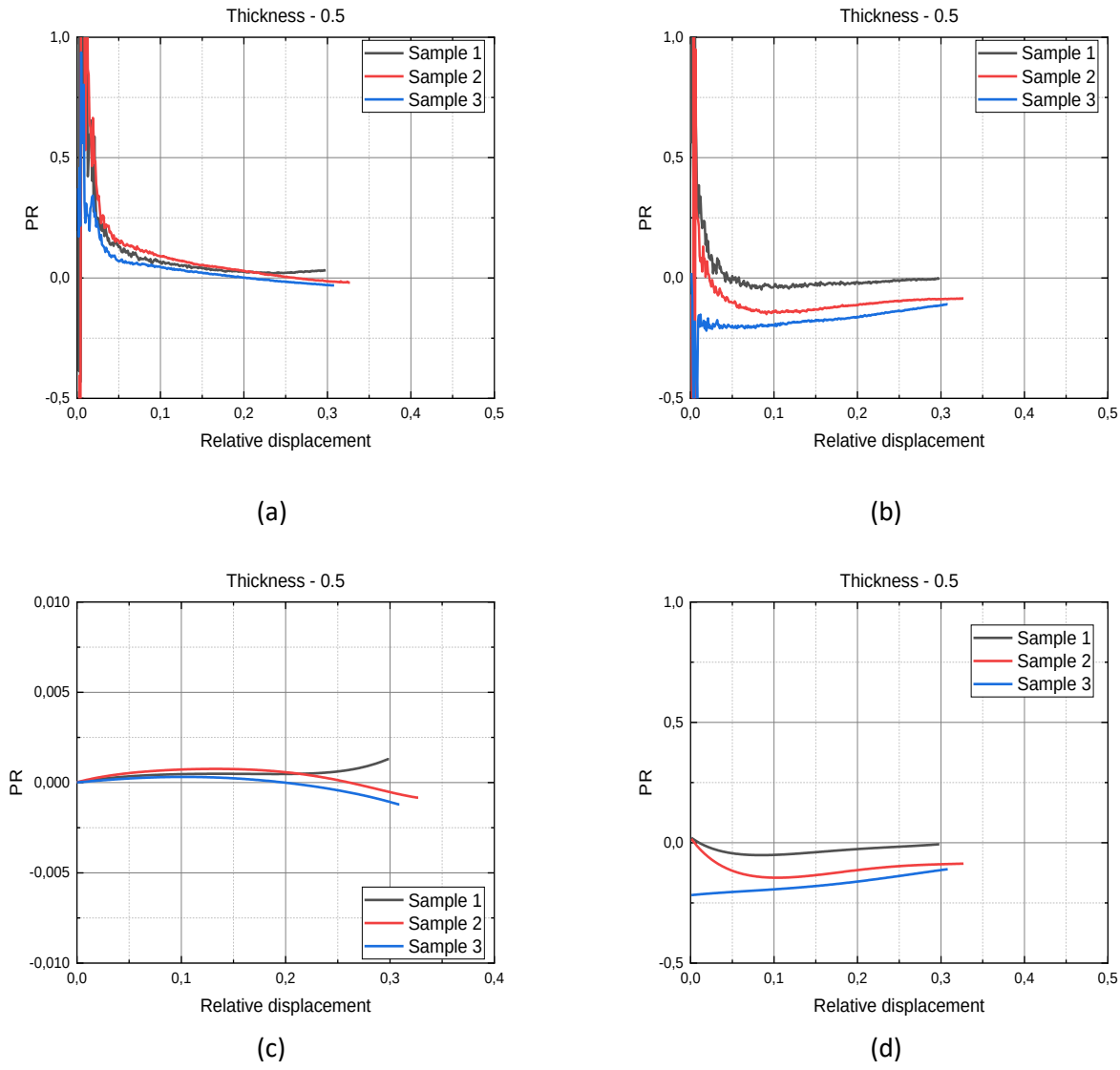

Figure 26 - PR / Relative displacement curves before (a,b) and after (c,d) fitting, for external (a,c) and internal (b,d) points, in a gyroid structure with a wall thickness of 0.5 mm.

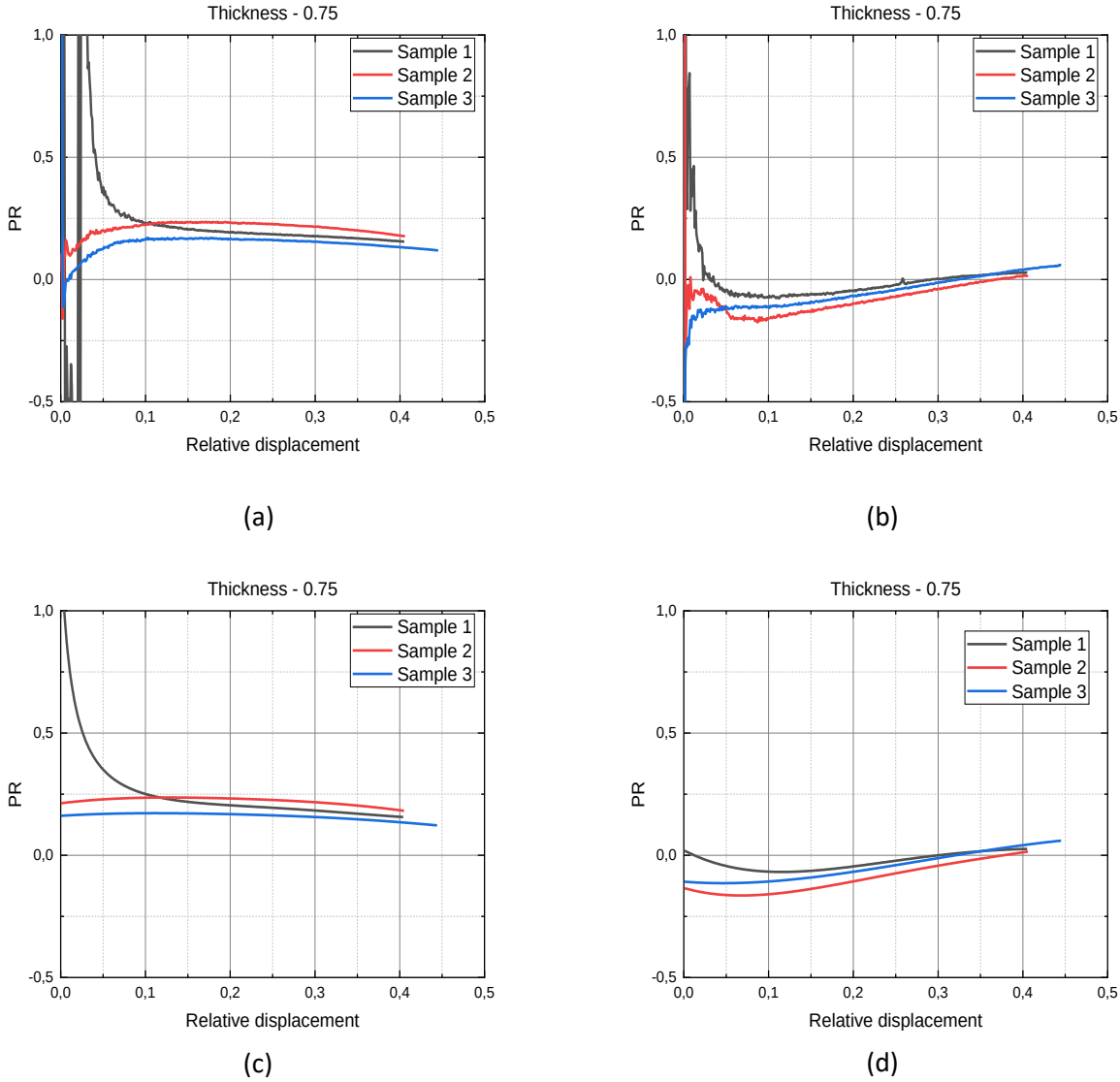

Figure 27 - PR / Relative displacement curves before (a,b) and after (c,d) fitting, for external (a,c) and internal (b,d) points, in a gyroid structure with a wall thickness of 0.75 mm.

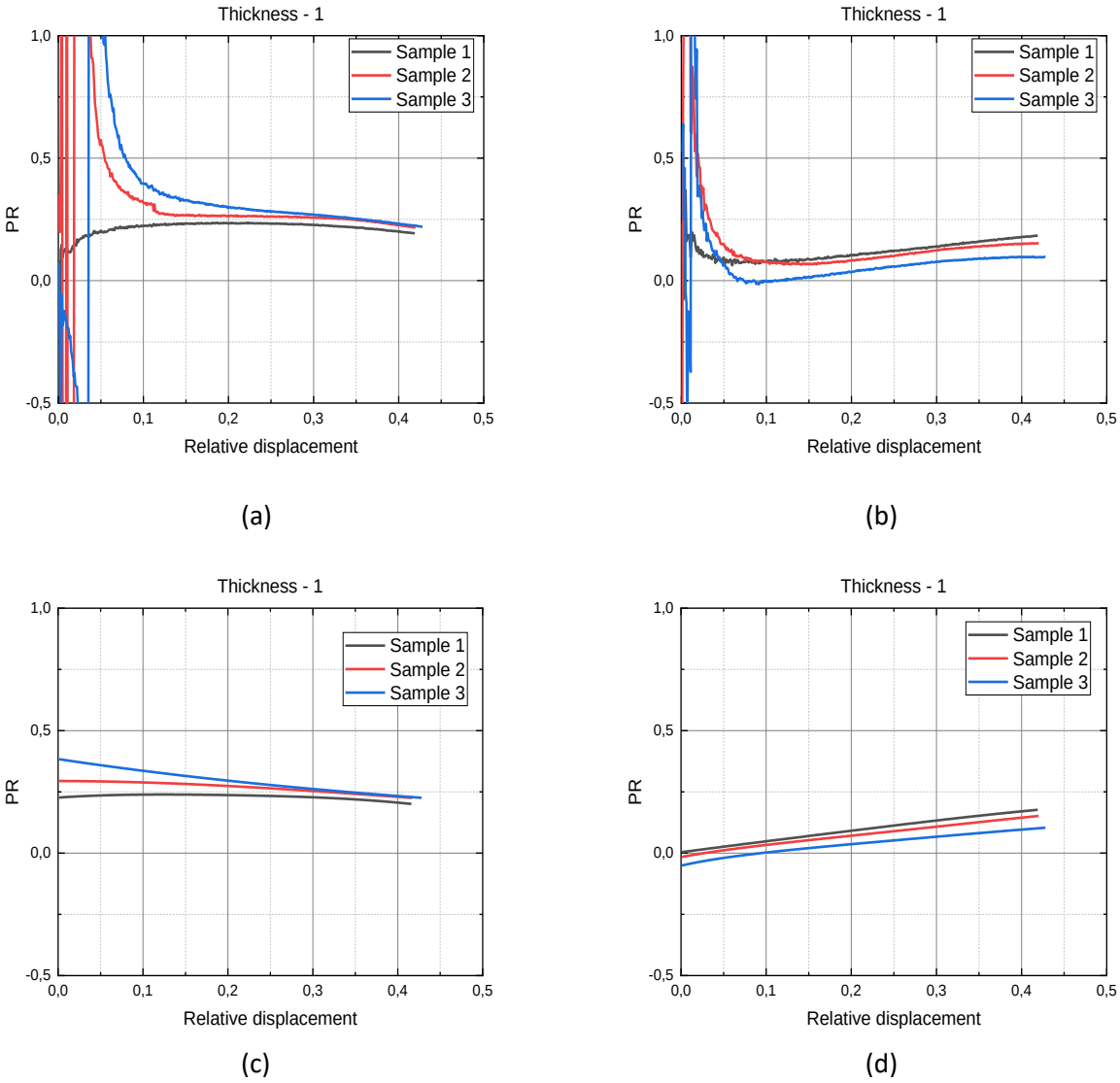

Figure 28 - PR / Relative displacement curves before (a,b) and after (c,d) fitting, for external (a,c) and internal (b,d) points, in a gyroid structure with a wall thickness of 1 mm.

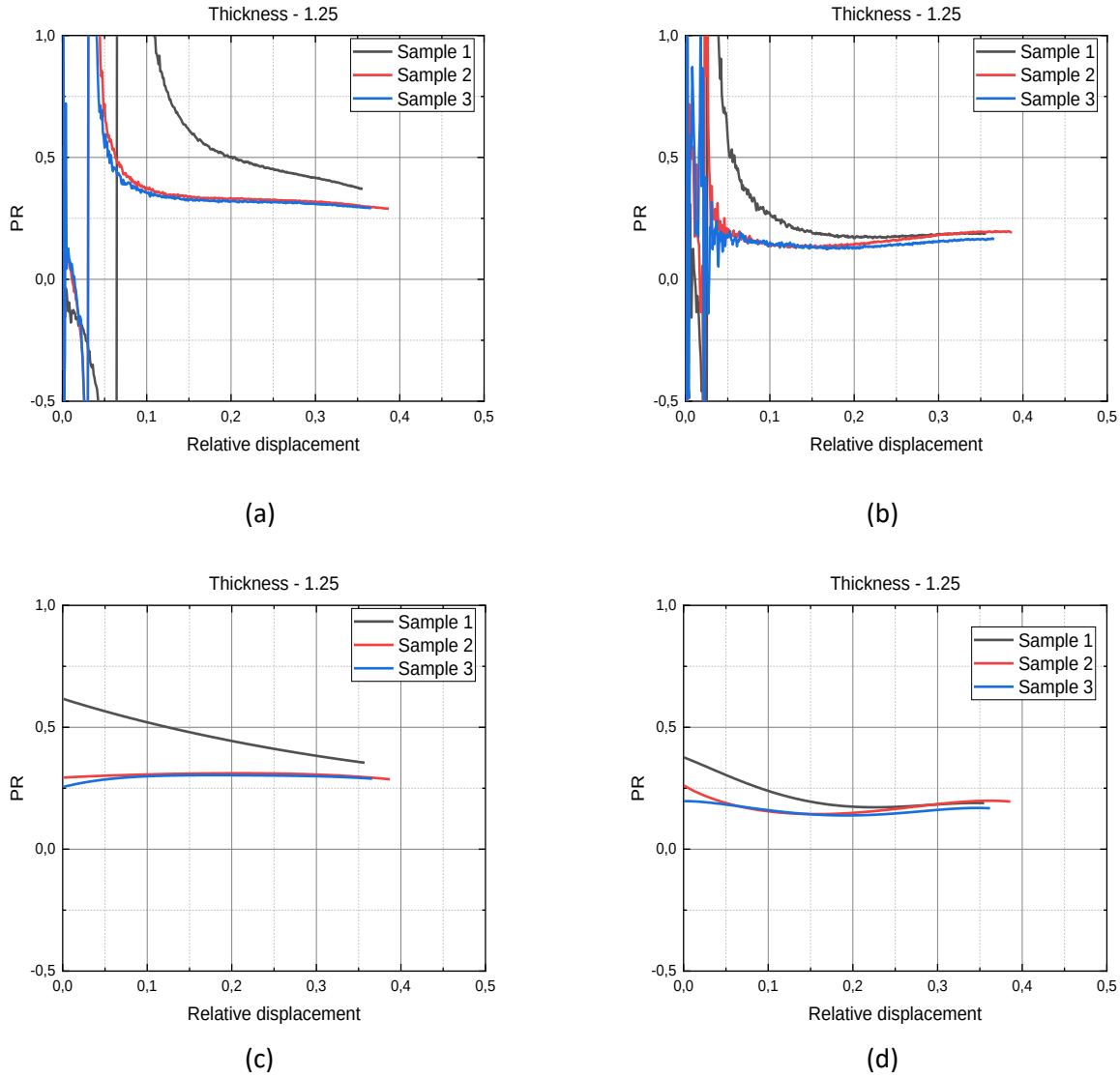

Figure 29 - PR / Relative displacement curves before (a,b) and after (c,d) fitting, for external (a,c) and internal (b,d) points, in a gyroid structure with a wall thickness of 1.25 mm.

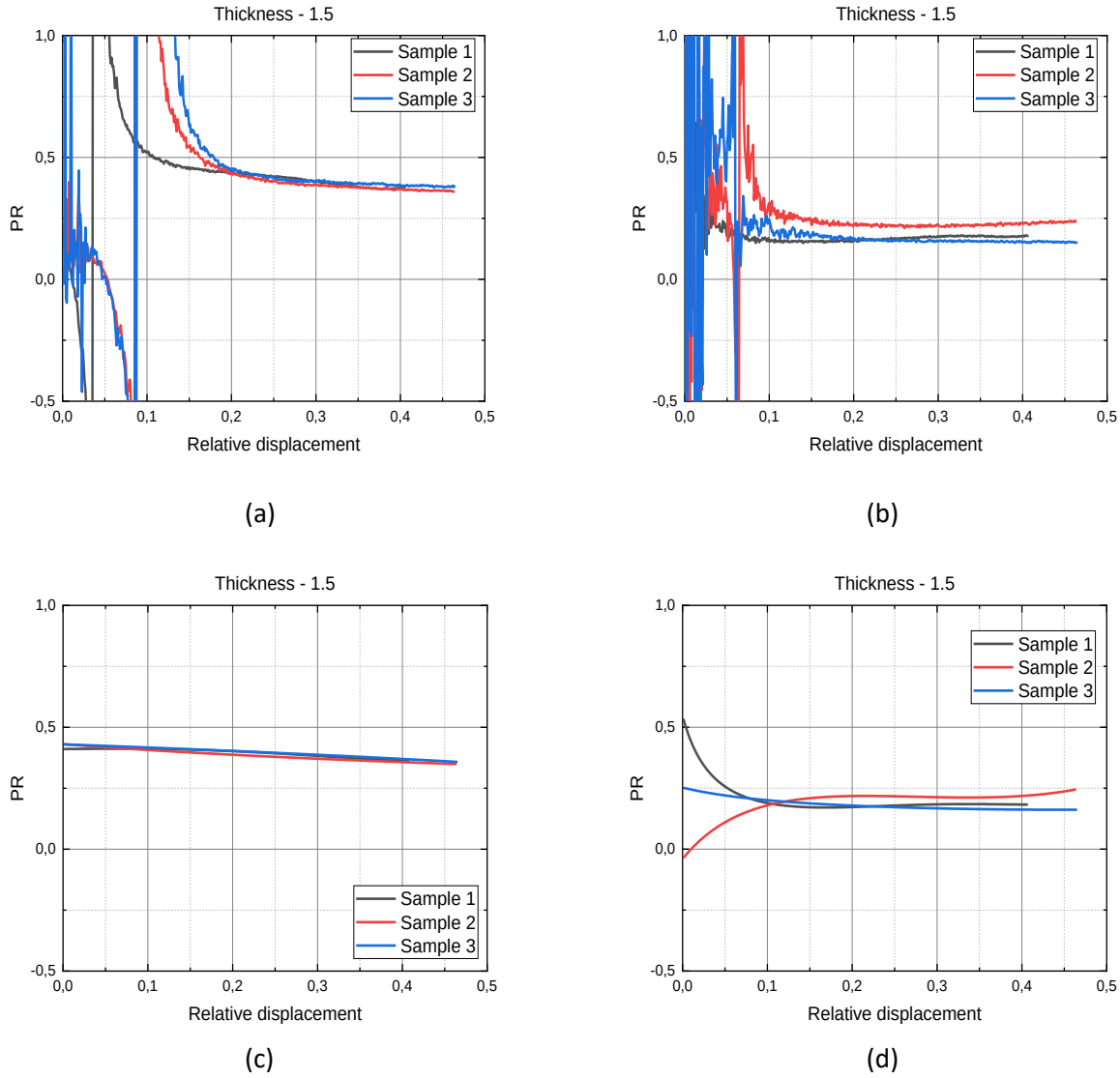

Figure 30 - PR / Relative displacement curves before (a,b) and after (c,d) fitting, for external (a,c) and internal (b,d) points, in a gyroid structure with a wall thickness of 1.5 mm.

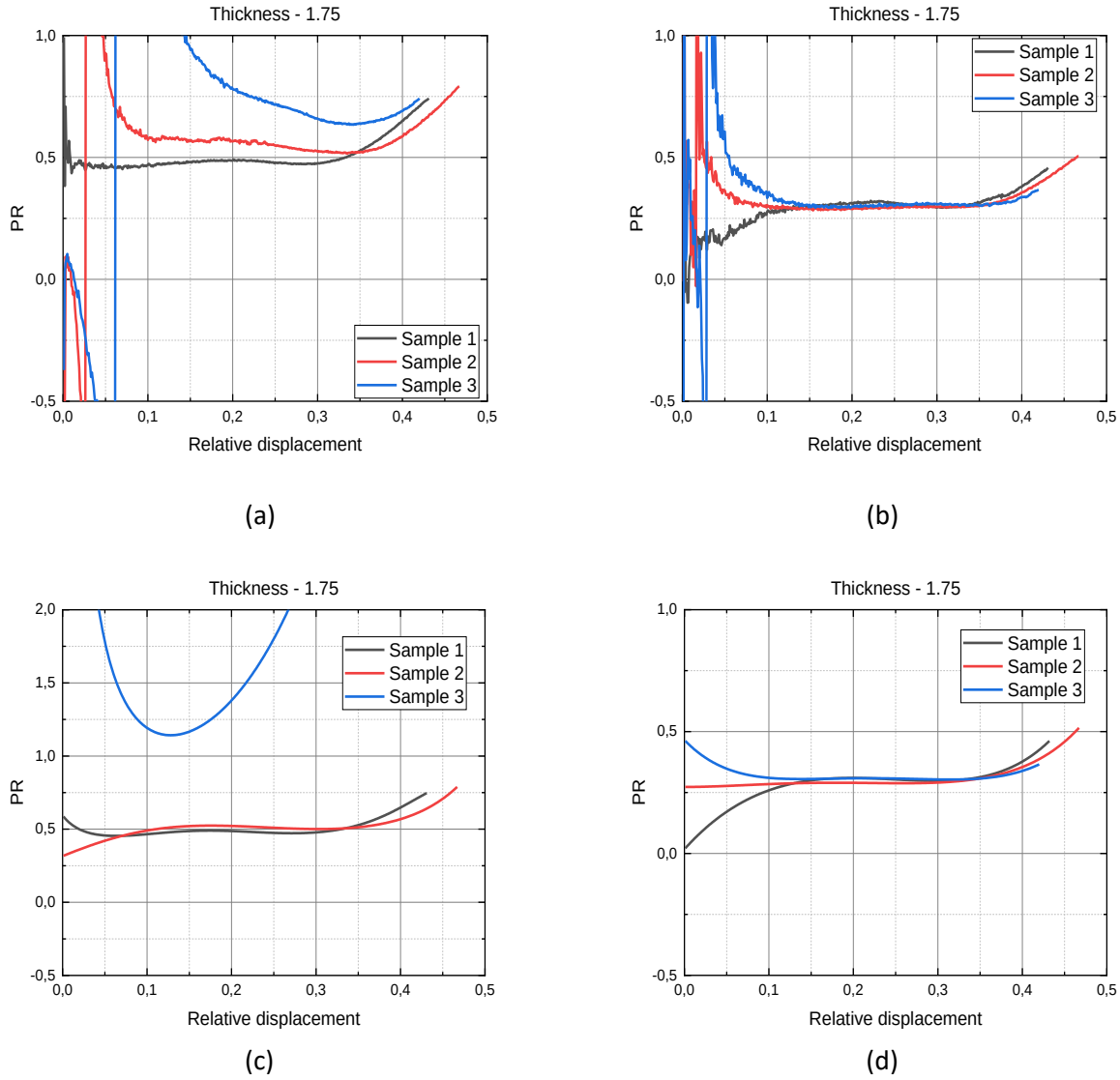

Figure 31 - PR / Relative displacement curves before (a,b) and after (c,d) fitting, for external (a,c) and internal (b,d) points, in a gyroid structure with a wall thickness of 1.75 mm.

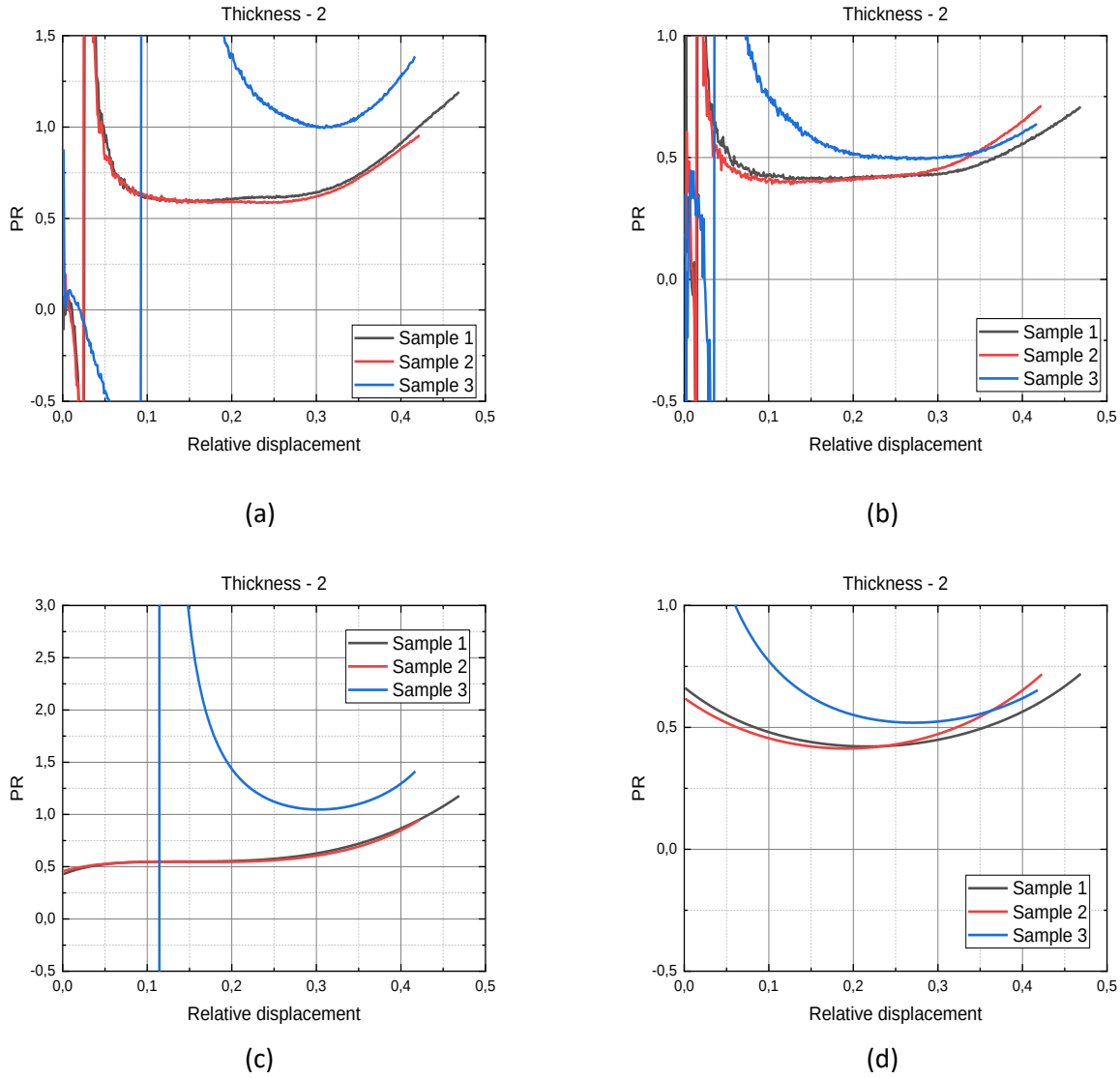

Figure 32 - PR / Relative displacement curves before (a,b) and after (c,d) fitting, for external (a,c) and internal (b,d) points, in a gyroid structure with a wall thickness of 2 mm.

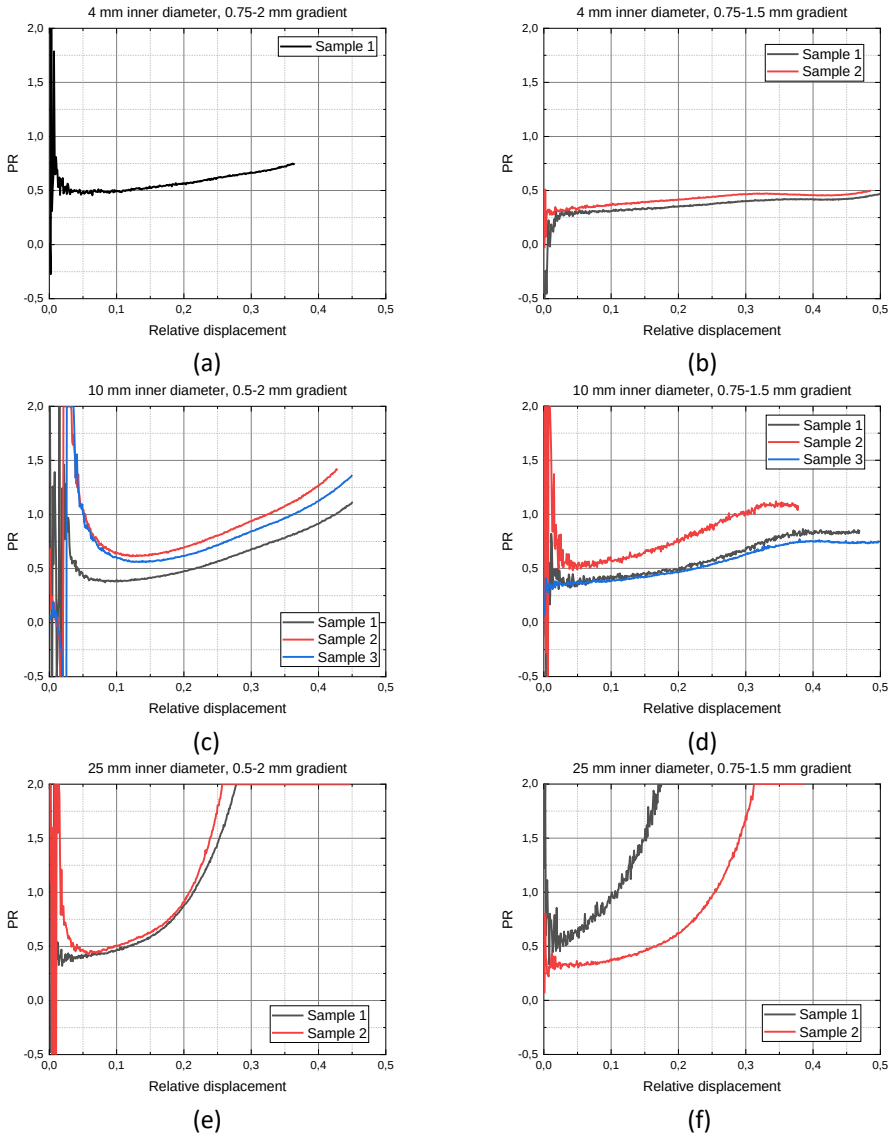

Figure 33 - PR / Relative displacement curves before fitting, for different inner diameters of 4 mm (a, b), 10 mm (c, d) and 25 mm (e, f) and wall thickness gradients of 0.75-2 mm (a), 0.5-2 mm (c, e), and 0.75-1.5 mm (b, d, f).

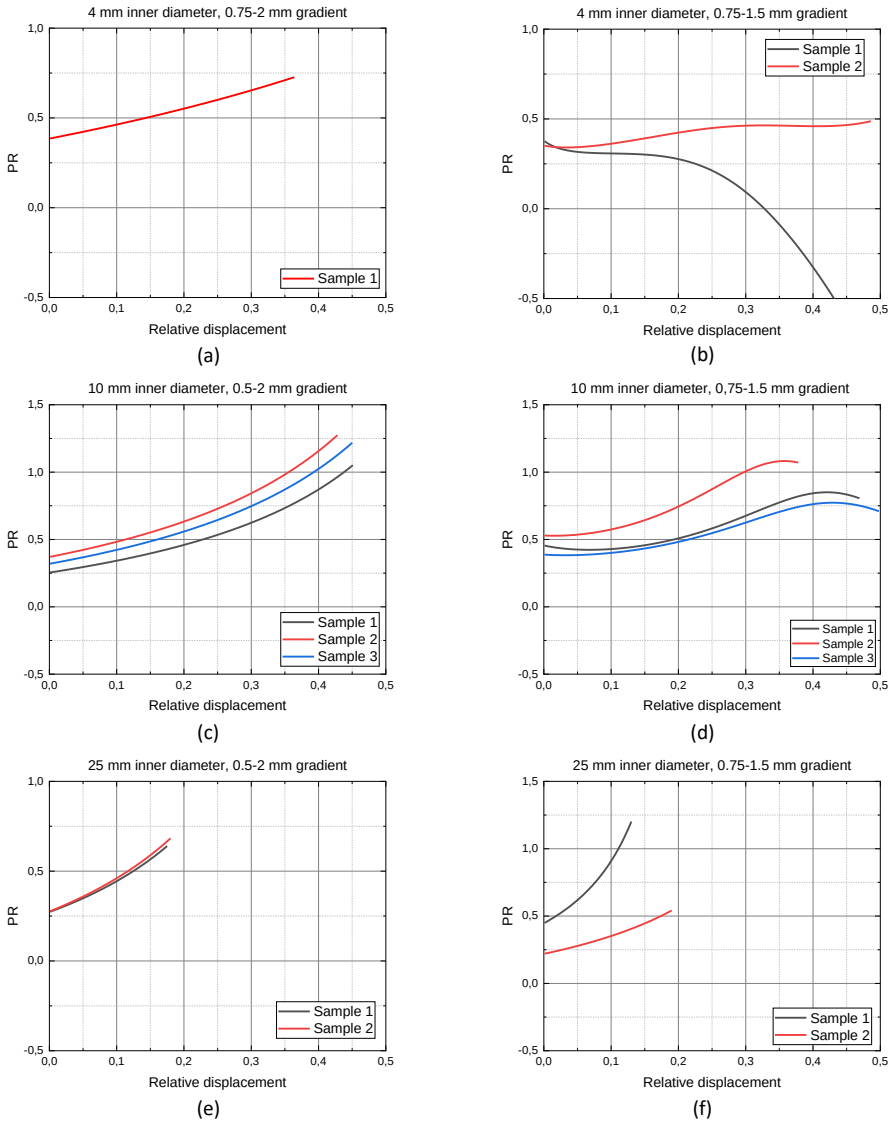

Figure 34 - PR / Relative displacement curves after fitting, for different inner diameters of 4 mm (a, b), 10 mm (c, d) and 25 mm (e, f) and wall thickness gradients of 0.75-2 mm (a), 0.5-2 mm (c, e), and 0.75-1.5 mm (b, d, f).